Altered ISGylation drives aberrant macrophage-dependent immune responses during SARS-CoV-2 infection

Sumana Sanyal (✉ sumana.sanyal@path.ox.ac.uk)
University of Oxford https://orcid.org/0000-0002-6230-5366

Horace Lee
University of Hong Kong

Deeksha Munnur
University of Oxford

Qi Teo
University of Hong Kong

Julian Ho
University of Hong Kong

Wilson Ng
University of Hong Kong

Lewis Siu
University of Hong Kong

Eric Spooner
Whitehead Institute for Biomedical Research

Hidde Ploegh
Harvard Medical School

Adan Pinto-Fernandez
University of Oxford

Andreas Damianou
University of Oxford

Benedikt Kessler
University of Oxford https://orcid.org/0000-0002-8160-2446

Chris Mok
The University of Hong Kong

Article

Keywords: ISG15, Ube1L, CCL2, IFN, Influenza, Zika, SARS-CoV-2, macrophages

Posted Date: September 10th, 2020

DOI: https://doi.org/10.21203/rs.3.rs-63942/v1

Version of Record: A version of this preprint was published at Nature Immunology on October 18th, 2021.
See the published version at https://doi.org/10.1038/s41590-021-01035-8.

Altered ISGylation drives aberrant macrophage-dependent immune responses during SARS-CoV-2 infection

Horace HY Lee[1#], Deeksha Munnur[2#], Qiwen Teo[1#], Julian Ho[1], Wilson WS Ng[1], Lewis YL Siu[1], Eric Spooner[3], Hidde Ploegh[4], Adan Pinto-Fernandez[5], Andreas Damianou[5], Benedikt Kessler[5], Sumana Sanyal[2,1*] and Chris Ka Pun Mok[1*]

[1]HKU-Pasteur Research Pole, School of Public Health, Li Ka Shing Faculty of Medicine, The University of Hong Kong, Hong Kong SAR, PR China

[2]Sir William Dunn School of Pathology, South Parks Road, University of Oxford, Oxford OX1 3RE, UK

[3]Whitehead Institute for Biomedical Research, Massachusetts Institute of Technology, Cambridge, MA, 02142, USA

[4]Boston Children's Hospital and Harvard Medical School, 50 Blossom Street, Boston, MA 02114, USA

[5]TDI Mass Spectrometry Laboratory, Target Discovery Institute, Nuffield Department of Medicine, University of Oxford, Oxford OX3 7FZ, UK

[#] equal contribution

***Correspondence author:**

Sumana Sanyal, Chris Ka Pun Mok

Email: sumana.sanyal@path.ox.ac.uk, ch02mkp@hku.hk

Keywords: ISG15, Ube1L, CCL2, IFN, Influenza, Zika, SARS-CoV-2, macrophages

Running title: ISGylation regulates macrophage responses

Abstract

Interferon stimulated gene 15 (ISG15) is a ubiquitin like modifier frequently induced during virus infections and involved in versatile host defense mechanisms. Not surprisingly, many viruses including SARS-CoV-2 have evolved de-ISGylating activities to antagonize its effect. In this study we compared ISG15-driven macrophage responses upon infection by influenza, Zika and SARS-CoV-2 viruses. ISG15 and its modifying enzymes were upregulated in human macrophages after infection with all three viruses. While influenza and Zika viruses induced cellular ISGylation, SARS-CoV-2 triggered hydrolysis of ISG15 modifications instead, to generate free, extracellular ISG15 from macrophages and dendritic cells, but not from bronchial epithelial cells. Extracellular ISG15 was released independent of the conventional secretory pathway or cell death, but instead, depended on a non-classical autophagy-related secretory process. Increase of extracellular ISG15 was also reflected in serum samples from COVID-19 patients. The high ratio of free versus conjugated ISG15 in SARS-CoV-2 infected cells triggered macrophage polarization towards a M1 phenotype, increased secretion of pro-inflammatory cytokines, e.g. MCP-1 (CCL2), IL-1β, TNFα and IL-6, and attenuated antigen presentation. Depleting ISG15 conjugating enzymes Ube1L and HERC5 further increased free ISG15 and exacerbated this effect. We could recapitulate this phenomenon by expressing the wild-type but not the catalytically inactive PLpro de-ISGylating enzyme of SARS-CoV-2. Proteomic analyses of the secretome from SARS-CoV-2 infected macrophages revealed that besides ISG15, it displayed significant enrichment in non-classical secretory proteins and inflammatory responses, which was further amplified by free ISG15. Collectively, our results indicate that increased proportions of free ISG15 dramatically alter macrophage responses and is likely a key feature of cytokine storms triggered by highly pathogenic respiratory viruses such as influenza and SARS-CoV-2.

Introduction

Viruses that cause acute infections of the human respiratory tract such as influenza and coronaviruses are responsible for high rates of morbidity and mortality. The seasonal flu is estimated to affect 3-5 million cases worldwide. The ongoing pandemic of SARS-CoV-2 has already affected >20 million people. Interferons (IFN) are the first line of defense against several pathogens [1]. They are produced and secreted by the host to boost innate immune responses. Many viruses activate type-I IFN (IFNα/β) signaling, which results in upregulation of a large group of interferon-stimulated genes (ISGs) that exert broad antiviral activities and contribute to lung inflammation [2,3]. Although hosts deficient in type-I IFN are more susceptible to virus infections [4], an excess of type-I IFN or aberrant cytokine response may lead to extensive lung damage and host death, as is commonly observed in highly pathogenic cases of influenza [5] and coronaviruses [67]. Mice lacking IFNα receptors (IFNAR) have a higher survival rate to influenza infection than wild-type animals [8], again pointing to a dysregulation of IFN signaling in the pathogenesis of severe cases.

Macrophages are cells of the innate immune system that play a critical role in modulating disease severity during virus infections. They can be infected by influenza and coronaviruses, and are the major producers of pro-inflammatory cytokines, such as TNFα, IFNβ, IP-10 (CXCL10), MCP-1 (CCL2), which have an impact on the pathogenesis and clinical outcomes in the host [9–12]. Regulation of cytokines in macrophages is essential. It has been proposed that overproduction of cytokines, commonly defined as “cytokine storms”, aggravates lung damage with uncontrolled extravasation of immune cells, including macrophages or monocytes into infection sites [6,13], although the exact sequence of events are not yet completely understood.

Interferon stimulated gene 15 (ISG15) is a ubiquitin-like modifier that is part of the first line of defense against pathogens, with broad-spectrum antiviral activity. Post translational modifications by ubiquitin and ISG15 are frequently targeted by viruses to perturb host immune responses [14]. ISG15 and its modifying enzymes are highly up-regulated by type-I IFN [15]. ISG15 can be conjugated (ISGylated) to other proteins in a process termed ISGylation or be secreted in its free form. Among the hundreds of modifiable substrates, many have immune-related functions [16–18], and ISG15 (free or conjugated) has been shown to protect the host against infections [19].

The function of ISG15 in virus infection has so far been investigated in influenza virus infected epithelial cells. ISG15 modified influenza NS1 protein inhibited virus

replication whereas modification of Tsg101, a member of the ESCRT complex inhibited transport of viral proteins [18,20–22]. Its impact in cells of the innate immune system such as macrophages is not known, with only one report suggesting that ISG15 in mice peritoneal macrophages is essential for influenza virus-triggered phagocytosis [23]. The fate of ISGylation in Zika or coronavirus-infected macrophages has not been reported so far.

In this study, we show that ISG15 and its modifying enzymes are upregulated in influenza, Zika and SARS-CoV-2 infected human macrophages. While influenza and Zika viruses triggered both cellular ISGylation and release of modest levels of free ISG15, infection by SARS-CoV-2 was able to reduce intracellular ISG15 conjugates while dramatically increasing secretion of free ISG15, a phenomenon reflected in serum samples from patients. The increased ratio of free to conjugated ISG15 in SARS-CoV-2 infected cells was accompanied by aberrant macrophage immune responses, which included polarization towards the M1 phenotype, secretion of pro-inflammatory cytokines, and downregulation of IFN-production and antigen presentation. Depletion of Ube1L or HERC5 that specifically prevented ISGylation and increased free ISG15, exacerbated the hyper-induction of pro-inflammatory cytokines such as MCP-1 (CCL2), IL-6, and IL-1β, without affecting virus replication. This effect was recapitulated by expressing the wild-type but not the catalytically inactive SARS-CoV-2 PLpro de-ISGylating enzyme alone, indicating that it is necessary and sufficient to dysregulate macrophage responses. We verified this phenomenon in a quantitative analysis of the secretome which revealed enrichment of non-classical secretory components and cytokine responses in SARS-CoV-2 infected macrophages. Collectively our data underscore the critical impact of altered free versus conjugated ISG15 on macrophage function, underpinning the onset of lymphopenia and cytokine storms during infections by highly pathogenic respiratory viruses.

Results

Virus infection induces bulk ISGylation in human macrophages

ISG15 is produced during virus infections downstream of Type-I IFNs [24,25]. Upregulation of ISG15 and modifying enzymes, including the E1 activating enzyme Ube1L, E2 conjugation enzyme UbcH8, E3 ligase HERC5, and de-ISGylase USP18, have been reported, albeit only in virus infected epithelial cells [20,26]. How these genes

120 are regulated in virus-infected human macrophages, is not well-understood. To
121 determine whether ISG15 and its modifying enzymes are expressed and upregulated
122 in virus infected macrophages, we performed RT-qPCR to quantify the mRNA levels
123 of ISG15, Ube1L (E1), UbcH8 (E2), HERC5 (E3), and USP18. We treated
124 macrophages with IFNβ as positive control, where ISG15 and the conjugating
125 enzymes were all induced as anticipated (**Fig 1a-i**). In those infected by human
126 influenza A (H1N1) or avian influenza A (H9N2) virus, expression of all mRNAs, with
127 the exception of Ube1L, was upregulated (**Fig 1a-e**). In those infected by either Zika
128 or SARS-CoV-2, both (+)RNA viruses, the fold-induction was comparable to that in
129 influenza infected cells (**Fig 1f-i**). Intracellular ISG15 protein, measured by ELISA, was
130 equivalently upregulated after infection by influenza and Zika viruses, and more
131 significantly with SARS-CoV-2 (**Fig 1j, k**). These results indicate that ISG15 and
132 modifying enzymes are expressed in macrophages and markedly induced following
133 virus infection.
134 ISG15 is a ubiquitin-like (Ubl) modifier that is known to exert its antiviral function
135 via post-translational modification of substrates [18]. In influenza-infected macrophages,
136 bulk ISGylation in cell lysates was detected for both avian (H9N2/Y280), mammalian-
137 adapted (H9N2/Y280-PB2-627K) or pandemic (H1N1/CA04) influenza strains (**Fig 1l**).
138 Similarly, cellular ISGylation was significantly induced in Zika-infected macrophages
139 (**Fig 1l**). Interestingly, although the conjugating enzymes were induced upon SARS-
140 CoV-2 infection, cellular ISGylation remained significantly low (**Fig 1l**), suggesting that
141 SARS-CoV-2 is able to trigger de-ISGylation of cellular substrates.
142 Although type-I IFN signaling is a well-known pathway that induces ISG15 and
143 ISGylating enzymes [18], type-I IFN independent mechanisms have also been proposed
144 [27,28]. For example, DNA damage by UV or genotoxic drugs could induce p53-mediated
145 expression of ISG15 and its modifying enzymes [28]. To investigate whether virus
146 infection-induced ISG15 expression was dependent on type-I IFN signaling, we
147 infected macrophages in the presence of neutralizing antibodies directed against type-
148 I IFN receptor (anti-IFNAR2) or isotypic control. ISG15 expression was determined by
149 RT-qPCR (**Fig S1a**) and Western blotting (**Fig S1b**). In the presence of anti-IFNAR,
150 ISG15 mRNA expression as well as free and conjugated ISG15 was diminished
151 compared to isotypic control, implying that this was primarily dependent on type-I IFN
152 signaling in macrophages.

Free ISG15 is secreted from virus-infected macrophages via unconventional mechanisms

Apart from its function as a Ubl protein modifier, ISG15 is also known to function as a free, non-conjugated protein [29], which can be secreted into the extracellular space [30]. Mice harboring a deletion of Ube1L (E1) (which abolishes ISGylation) survived better than ISG15$^{-/-}$ (which abolishes both free and conjugated ISG15) animals, suggesting that both free and conjugated forms of ISG15 play protective roles in virus infections [19]. We were able to detect extracellular ISG15 after infection by each of the viruses, but not from cells stimulated by type-I IFN (**Fig 2a**). Highest amounts of secreted ISG15 was detected from SARS-CoV-2 infected cells (**Fig 2b**). In contrast, infection with UV-inactivated Zika or SARS-CoV-2 did not trigger secretion of ISG15 at all, indicating that live virus is necessary for this process (**Fig 2c**).

The process of ISG15 secretion is not well characterized and has been proposed to occur from granulocytes via unconventional mechanisms [31,32]. To assess its mode of secretion from virus-infected macrophages, we used Brefeldin A treatment to block the conventional secretory pathway (**Fig 2d, e**). Brefeldin A treatment did not affect secretion (**Fig 2d**), nor did it appreciably alter intracellular levels of ISG15 (**Fig 2e**), indicating that it is likely secreted via unconventional mechanisms. We also treated cells with caspase inhibitors to block cell death (**Fig 2g**). Cell viability of mock and influenza virus-infected macrophages was virtually identical (**Fig 2f**), and inhibition of caspases with Z-YVAD-FMK and Z-DEVD-FMK did not have any significant effect on ISG15 secretion (**Fig 2g**), indicating that it is not dependent on the activation of apoptotic or necrotic pathways. Instead, depleting components of secretory autophagosomes/lysosomes [33] abolished ISG15 secretion (**Fig 2h, i, S2a-b**). Collectively, these data indicate that virus-infections can specifically trigger secretion of free ISG15 via autophagy-dependent unconventional mechanisms, with the highest amounts detected from SARS-CoV-2 infected macrophages.

Free ISG15 is specifically secreted by monocytic cells during virus infections

Epithelial cells, macrophages and dendritic cells (DCs) in the respiratory tract are all essential infection targets of influenza and coronaviruses [34,35]. On the other hand, Zika displays broad tissue tropism including monocytes, monocyte-derived macrophages and dendritic cells as well as neural cells and hepatocytes [36]. The tissue tropism of

SARS-CoV-2 is less well understood; however, both lung epithelial cells and macrophages get infected, although replication in macrophages appears to be limited [37]. We detected a comparable extent of influenza virus replication and induction of ISG15 mRNA expression in Normal Human Bronchial Epithelial (NHBE), DCs, and macrophages (**Fig 3a, b**). Secretion of ISG15 was however detectable only from DCs and macrophages, with the highest amounts from the latter (**Fig 3c**). These observations were not limited to the avian influenza virus strain used. Human influenza virus (H1N1/WSN), could also replicate in all three cell types and enhance ISG15 gene expression, but triggered ISG15 secretion only from macrophages and dendritic cells (**Fig 3a-c**). This phenomenon was also recapitulated in Zika and SARS-CoV-2 infected iPSC-derived macrophages and DCs. Despite comparable replication among the different cell types, secretion of ISG15 occurred from macrophages and DCs infected with either SARS-CoV-2 or with Zika virus (**Fig 3d, e**), with the highest amounts released from SARS-CoV-2 infected macrophages (**Fig 3f**). These results indicate that respiratory viruses such as influenza and coronaviruses both of which have the potential to cause “cytokine storms” trigger secretion of ISG15 from immune cells to a significantly greater extent compared to Zika virus, which is well-adapted to replicate in macrophages and therefore likely able to circumvent macrophage-mediated immune responses.

SARS-CoV-2 infection triggers aberrant immune responses in macrophages

The dramatically reduced ISGylation (**Fig 1**) and increase in secreted ISG15 (**Fig 2**) from SARS-CoV-2 infected macrophages prompted us to investigate the general macrophage immune responses in SARS-CoV-2 infection. Clinical samples from Covid-19 patients have already indicated aberrant early immune responses in SARS-CoV-2 infection, often accompanied by lymphopenia and secretion of pro-inflammatory cytokines [38,7]. We infected iPSC-derived macrophages with SARS-CoV-2 at MOI 2. At 24h post infection, surface presentation of both MHC-I and MHC-II was significantly downregulated specifically in the virus-infected population, but not with UV-inactivated virus control or with dsRNA transfection, a phenomenon that was also evident in Zika-infected cells (**Fig 4a, 4b, S3a, S3b**). To assess other immune responses, we measured macrophage polarization, cytokine secretion profiles and phagocytic activity (**Fig 4c-e**). Polarization was measured in iPSC-derived macrophages infected with SARS-CoV-2 and markers compared with those that were either differentiated into an

M1 state using M-CSF, LPS and IFN-γ or an M2-state using M-CSF and IL-4 (**Fig 4c**). SARS-CoV-2 infected macrophages displayed a strong M1-like pro-inflammatory phenotype (**Fig 4c**). We also measured induction of a selected set of cytokines which have been reported to be altered in SARS-CoV-2 infection. Secretion of pro-inflammatory cytokines such as IL-1β, MCP-1 and IL-6 was significantly upregulated in SARS-CoV-2 infection. On the other hand, that of IFN-I and IFN-II was significantly downregulated, recapitulating the clinical pathology in COVID-19 patients (**Fig 4d**). Similarly, phagocytic activity of SARS-CoV-2 infected macrophages resembled reduced activity observed in M1- but not M2-macrophages (**Fig 4e**). Collectively, these data indicate that infection by SARS-CoV-2 results in aberrant macrophage responses, downregulating antigen presentation and triggering secretion of inflammatory cytokines, which might underpin the consistent symptoms of lymphopenia and cytokine storm observed in Covid-19 patients.

Increasing ratio of free versus conjugated ISG15 drives pro-inflammatory cytokine responses from virus infected macrophages

To decouple the role of ISGylation from free ISG15 in virus-infected macrophages, we systematically knocked-down ISG15, Ube1L, HERC5 and USP18 by transfecting macrophages with DsiRNAs 72 hours prior to infecting with either H9N2/Y280, Zika or SARS-CoV-2 virus as specified. Knockdown efficiency of ISG15 and its modifying enzymes was verified in IFN-I treated cells by immunoblotting. The results confirmed that all DsiRNA targets were significantly depleted in comparison to control cells (**Fig 5a, S4a-c**). In ISG15 knockdown cells, as predicted, both free and ISGylated forms were downregulated, whereas in Ube1L and HERC5 knockdown cells, only the conjugated forms were downregulated (**Fig 5b**). USP18 is the cellular de-ISGylating enzyme and a negative regulator of type-I IFN response; as anticipated, we observed an upregulation of ISGylated material in USP18-depleted macrophages (**Fig 5b**). Depletion of either ISG15, ISGylating enzymes, or USP18 did not have any significant effect on replication of influenza, Zika or SARS-CoV-2 in macrophages (**Fig 5c**). In contrast, depletion of ISGylation alone, but not ISG15, stimulated secretion of pro-inflammatory cytokines, particularly MCP-1, IL-6 and IL-1β from virus-infected cells in general (**Fig 5d-f**), but most significantly from SARS-CoV-2 infected cells (**Fig 5f**). Interestingly, production of IFN-I and II from Zika and SARS-CoV-2 infected macrophages displayed the reverse effect. Cells depleted in ISG15 conjugating

enzymes did not have any significant effect on IFN-I or II production, whereas USP18-depleted cells displayed a modest increase (**Fig 5f**). Depletion of ISG15 and Ube1L/HERC5 but not USP18 also resulted in reduced phagocytic activity in virus-infected macrophages, indicating that ISGylation is important for this effector function of macrophages as reported previously (**Fig S5a, b**). Collectively, these data indicate that skewing the ratio towards a higher proportion of free ISG15 to its conjugated form drives hyperproduction of pro-inflammatory cytokines often detected in severe respiratory infections.

SARS-CoV-2 PLpro de-ISGylase can recapitulate aberrant macrophage phenotype of SARS-CoV-2 infection

A number of viruses including coronaviruses encode deubiquitylases and de-ISGylases in their genome. To evaluate whether expressing the viral de-ISGylase itself was sufficient to induce aberrant macrophage responses, we expressed the wild-type and catalytically inactive SARS-CoV-2 PLpro in iPSC-derived macrophages (**Fig 6a, b**). We measured cellular ISGylation upon IFN-I treatment in cells expressing either the empty control vector or those expressing either the wild-type or the mutant variants of PLpro. Dose-dependent expression of the wild-type, but not the mutant PLpro resulted in hydrolysis of bulk cellular ISGylation and a concomitant increase in free ISG15 in IFN-I treated cells, indicating that it is indeed an active de-ISGylase (**Fig 6c**). To investigate whether the PLpro enzyme was sufficient to alter macrophage responses, we measured surface expression of MHC-I and secretion of the panel of cytokines described in Fig 5 in cells transfected with dsRNA. Expression of the wild-type but not the mutant PLpro was able to recapitulate downregulation of MHC-I presentation (**Fig 6d, e**). Expression of the wild type and catalytically mutant variants of USP18 - the cellular de-ISGylase – confirmed the ISGylation-dependent downregulation of MHC-I (**Fig 6f, g**). PLpro-expressing cells displayed increased secretion of pro-inflammatory cytokines such as MCP-1, IL-6, TNFα and IL-1β along with free ISG15, and attenuated secretion of IFN-I and II (**Fig 6h, i**). To validate our findings in clinical settings we collected serum samples from patients, which also displayed increased amounts of free ISG15 at their first week of disease onset (**Fig 6j**). Collectively, the results suggest that the de-ISGylating activity encoded by SARS-CoV-2 can disrupt early immune responses in macrophages which likely underpin the severe lymphopenia and cytokine storm that often accompanies severe COVID-19.

Quantitative analyses of ISG15-dependent responses in SARS-CoV-2 infected macrophages

Aberrant cytokine responses from PLpro expressing cells prompted us to systematically analyse the ISG15-dependent secretome from SARS-CoV-2 infected macrophages and compare that with IFNγ treated macrophages as shown in schematic (**Fig 7a**). We performed a quantitative mass spectrometry based proteomic analysis of the extracellular protein profile (secretome) of SARS-CoV-2 infected and IFNγ treated macrophages using established strategies of label free quantitation. We selected 24 h post SARS-CoV-2 infection or IFNγ treatment as the timepoint for analyses in macrophages expressing non-targeting (NT) DsiRNA or those targeting ISG15 or Ube1L. We defined the secretome as proteins released via all mechanisms, including classical, non-classical and exosomal pathways. Using LC-MS/MS mass spectrometry and MaxQuant proteomics software package for computational analyses we detected relative protein abundances in the conditioned media of control, SARS-CoV-2 infected or IFNγ treated macrophages. For increased confidence in the protein identification numbers we required that a protein be identified on the basis of at least two unique peptides and quantified in a minimum of two replicates.

We identified 489, 428 and 502 protein in IFNγ treated NT, ISG15-deficient and Ube1L-deficient macrophages, whereas 508, 485 and 544 proteins in SARS-CoV-2 infected macrophages (**Fig 7b**). Principal component analysis of the secretome response in the NT, ISG15-deficient and Ube1L-deficient cells showed a clear separation of the ISG15-deficient cells from NT and Ube1L-deficient cells, which clustered together (**Fig 7c**). For the secretome data sets, the first three principal components captured 89% (PC1: 51%, PC2: 25%, PC3: 13%) variability in the data. Pairwise comparison showed the highest overlap between NT and Ube1L-deficient SARS-CoV-2 infected macrophages. We evaluated the responses of the common proteins identified in all the conditions. Hierarchical clustering analyses of these common proteins revealed that the secretome of NT and Ube1L-deficient clustered together while that of ISG15-deficient cells was significantly different from the others (**Fig 7d**). Functional enrichment analyses revealed that the most prominent enrichment in the secretome of SARS-CoV-2 infected cells were of the inflammatory responses, cytokine secretion, non-classical secretory processes and exosomes, which strongly correlated specifically with Ube1L-deficient cells that inhibited the conjugated but not the extracellular free form of ISG15 (**Fig 7e**). These data therefore provide a systematic

overview of the core macrophage processes regulated by cellular ISG15 in response to SARS-CoV-2 infection.

Discussion

In-vitro and in-vivo studies have established that macrophages are one of the major determinants of pathogenesis during respiratory virus infections [39–42], driven by the production of interferons and interferon stimulated genes. However, the role of ISG15 in its free or conjugated form, in macrophage-mediated immune responses is not well studied. Here, we compared the ISG15-dependent responses of human macrophages to influenza, Zika and SARS-CoV-2 virus infections. All these viruses transcriptionally upregulated ISG15 and ISGylating enzymes, which was accompanied by increased bulk protein ISGylation in influenza and Zika, but not in SARS-CoV-2 infected cells. This is particularly intriguing since SARS-CoV-2 encodes for a papain-like protease (PLpro), which is a putative de-ISGylase. SARS-CoV-2 infected cells displayed a skewed ratio of free versus conjugated ISG15, accompanied by heightened secretion of pro-inflammatory cytokines despite reduced IFN production and antigen presentation. This phenomenon was exacerbated by depleting ISG15 conjugating enzymes Ube1L or HERC5, which prevented substrate ISGylation but not free ISG15. These data suggest that ISG15 regulates macrophage inflammatory responses either via protein ISGylation to inhibit secretory processes or via free ISG15 signaling that may induce cytokine production, or a combination of the two.

Secretion of ISG15 was specific to virus-infected antigen presenting cells, but not epithelial cells, consistent with its role in immune modulation. Extracellular free ISG15 can act as an adjuvant for $CD8^+$ cytotoxic T-cells [43] and can also influence infiltration or activation of immune cells such as neutrophils [44–46]. Early recruitment of NK and cytotoxic $CD8^+$ T-cells is vital to the host to control virus infection as well as lung inflammation [47–49]. Other reported immunomodulatory activities of extracellular ISG15 include anti-tumor activities of dendritic cells (DCs) [50], and triggering Type-II IFN response in NK and T-cells essential for immunity against mycobacteria [51].

Our results demonstrate that the combined effect of substrate-modified and free form of ISG15 critically affect the global immune response of macrophages during virus infections, unlike the respiratory tract epithelial cells where ISG15 primarily functions as an antiviral factor to limit viral replication [20–22]. Depletion of Ube1L or HERC5 that specifically prevented the conjugated, but not free ISG15, stimulated secretion of pro-

inflammatory cytokines from virus infected macrophages, such as MCP-1, TNFα, IL-6, all of which have been implicated in the cytokine storm caused by highly pathogenic influenza and severe Covid-19. MCP-1 (CCL2) and IL-6 have been consistently found to be a predictor of severe pathogenesis in respiratory virus infections. Uncontrolled MCP-1 secretion has also been implicated in increasing the severity of inflammatory disorders of the lung [52] and can regulate infiltration of immune cells, including monocytes, T-cells and NK cells [53]. Mice treated with pioglitazone, an agonist of the peroxisome proliferator-activated receptor-γ (PPAR-γ), was shown to reduce morbidity and mortality associated with influenza virus infection, correlated with reduced MCP-1 secretion [54]. Blocking MCP-1 can also reduce immune cell infiltration and ameliorate influenza pathogenesis in a viral replication independent manner [55]. We previously found that, in an in vivo mouse model, more pathogenic strains of influenza virus tend to induce a higher amount of MCP-1 [56]. More recently anti-IL-6 therapy has proved to be beneficial for treating severe COVID-19 cases [57].

Knockdown experiments also demonstrated that ISGylation is required to trigger macrophage effector functions in virus-infected human macrophages. We found that knockdown of ISG15 and Ube1L resulted in downregulation of phagocytic activities in human macrophages, in line with previous studies in mouse peritoneal macrophages [23].

Several viruses encode deubiquitylating and de-ISGylating activities in their genome that can counter host antiviral immunity. SARS-CoV-2 itself encodes a papain like protease which is a putative de-ISGylase [58]. Our data indicate that infection by SARS-CoV-2 removes ISG15 modifications from cellular substrates, confirming its intrinsic de-ISGylating ability. Reduced substrate ISGylation and increased free ISG15 was accompanied by hyperactivation of pro-inflammatory cytokines and reduced antigen presentation, both of which are key features of severe COVID-19. Expression of the wild-type but not catalytically inactive SARS-CoV-2 PLpro alone was able to trigger dramatic cellular de-ISGylation, recapitulating these results. Collectively, these data indicate that SARS-CoV-2 PLpro is able to perturb immune responses in macrophages, which may underpin the loss of CD8+ T-lymphocytes and increased inflammation often seen in severe COVID-19 [7].

Here we have characterized the role of ISG15 in virus-infected macrophages, which underscore the importance that the conjugated and free form plays in driving immune responses. Further characterization of the separable biochemical functions in animal models are called for to assess the specific core functions of ISG15 in response

to infections. Delineating the roles of free and conjugated forms of ISG15 should provide a better understanding of the pro- and antiviral impact of ISG15 in virus pathogenesis and ascertain whether aberrant ISG15-dependent macrophage effector responses underpin the cytokine storm and lymphopenia in COVID-19.

Materials and Methods

Plasmid Construction

The papain-like protease domain sequence is obtained from the SARS-CoV-2 complete genome (NCBI genome databank; NC_045512.2). Protein sequence for PLpro domain (amino acids, 746-1059) of pDONR207 SARS-CoV-2 Nsp3 (Addgene; #141257) was cloned into pCAGGs vector with C-terminal Flag-tag. Catalytic mutant (C117A) was generated by site-mutation PCR and verified with sequencing.

Virus cultures

Influenza virus gene segments were amplified by PCR using Pfu Turbo DNA polymerase (Stratagene Cat#600250) and cloned into pHW2000 vector (a gift from Robert G. Webster, St. Jude Children's Research Hospital). Individual plasmids containing the eight viral genome segments were co-transfected using TransIT-LT1 (MIR2300, Mirus Bio) into 293T (ATCC Cat#CRL-3216, RRID:CVCL_0063)/MDCK (ATCC Cat#CCL-34, RRID:CVCL_0422) co-cultures. Recombinant viruses generated from the transfection system were propagated in embryonated eggs and quantified by plaque assay. Zika virus (strain MR766) and SARS-CoV-2 stocks were prepared by determining tissue culture infective dose 50% ($TCID_{50}$/ml) in Vero E6 cells challenged with 10-fold serial dilutions of infectious supernatants for 90 min at 37ºC. Cells were subsequently incubated in DMEM with 2.5% FCS.

Primary cell culture and preparation for infection

Buffy coat packs from healthy donors were kindly provided by the Hong Kong Red Cross Blood Transfusion Service and autologous plasma was collected following centrifugation from the top layer. The study received ethical approval from the Institutional Review Board of the LKS Faculty of Medicine of the University of Hong Kong (Ref no: UW 17-050). The remaining portion was mixed with RPMI1640 medium (GIBCO Cat#23400021), overlaid onto Ficoll-Paque Plus density medium (GE

Healthcare Life Sciences Cat#17144003) and centrifuged at 1,000 x g for 20 minutes without braking. Peripheral blood mononuclear cells (PBMCs) were collected from the media-Ficoll interface. Plastic-adherent monocytes were cultured in 5% heat-inactivated autologous plasma in RPMI1640 medium and allowed to differentiate for 14 days into macrophages. For dendritic cells differentiation, 50ng/mL GM-CSF (Peprotech Cat#300-03), 10ng/mL IL-4 (Peprotech Cat#200-04), 5% heat-inactivated autologous plasma in RPMI1640 medium were used. Normal human bronchial epithelial cells (NHBE) were cultured in BEGM BulletKit Growth Media (Lonza Cat#CC-3170). The day before influenza virus infection, cells were harvested in trypsin/EDTA and 0.1 x 10^6 cells were seeded in 24-well cell culture plates (TPP).

iPSC-derived macrophages

iPSC-derived CD14+ monocytes generated from skin fibroblasts (from ATCC) were resuspended in macrophage differentiation base medium (RPMI 1640; 10% heat inactivated fetal calf serum, 2 mM L-glutamine; 100U/ml penicillin/streptomycin) supplemented with 100 ng/ml M-CSF. Cells were counted and seeded at a density of 150,000 precursor cells/well of a 6-well plate. Cells were cultured at 37ºC for 6 days to differentiate into mature macrophages. At day 7, cell density was verified to be 2-3 times that of initial number of precursors. Mature differentiated macrophages were infected with either Zika or SARS-CoV-2 for downstream functional assays.

Collection of plasma samples

Patients with RT-PCR confirmed COVID-19 disease at the Infectious Disease Centre of the Princess Margaret Hospital, Hong Kong, were invited to participate in the study after providing informed consent. The study was approved by the institutional review board of the Hong Kong West Cluster of the Hospital Authority of Hong Kong (approval number: UW20-169). Day 1 of clinical onset was defined as the first day of the appearance of clinical symptoms. Specimens of heparinized blood were collected from the patients, and the plasma were separated by centrifugation. The plasma was then heat inactivated at 56°C for 30 minutes and stored at -80°C until use.

Virus infection

Cells were infected with the indicated strains of viruses at 37°C in the corresponding culture medium under serum-free condition for 1 hour. The virus inoculum was then removed, cells were washed with warm PBS, and replenished with medium

supplemented with 100U/ml penicillin, 100µg/ml streptomycin (GIBCO Cat#15140122), and 1 µg/L TPCK-treated trypsin (Sigma Cat#T1426) in case of influenza.

Gene silencing by RNA interference

All gene-specific Dicer-substrate small interfering RNA (DsiRNA) oligos were purchased from IDT. DsiRNA was transfected with Viromer BLUE transfection reagent (Lipocalyx Cat#VB-01LB-01) at a final concentration of 25nM. Forty-eight hours post-transfection, cells were either harvested for analysis or subjected to additional experimental procedures as described.

Western blotting

Cells in 24-well plates were lysed on ice for 15 minutes in 100µl PBS pH 7.4, containing 1% IGEPAL and complete protease inhibitor cocktail (Roche). Following brief centrifugation (10 minutes at 13,000 x g), cleared lysates were separated by SDS-PAGE (12%) and proteins were transferred to PVDF membranes for Western blotting with anti-ISG15 (Boston Biochem Cat#A-830) and anti-GAPDH (Abcam Cat#ab8245, RRID:AB_2107448) antibodies, followed by horseradish peroxidase (HRP)-conjugated secondary antibody (Jackson ImmunoResearch Cat#115-035-003, RRID:AB_10015289). Protein bands were visualized by ECL™ Prime Western Blotting System (GE Healthcare Life Sciences Cat#RPN2232) using the Image Quant LAS 4000 mini machine (GE Healthcare Life Sciences).

ELISA

Cellular and secreted ISG15 were quantified with human ISG15 ELISA kit (MBL Cat#CY-8085) according to the manufacturer's instructions. Briefly, 100µL of cleared cell lysate or culture medium were captured on ELISA assay plates coated with anti-ISG15 antibody. After extensive washing in buffer containing 0.2% Tween, 100µL HRP-anti-ISG15 antibody was added for ISG15 protein detection. Binding was visualized by adding 100µL of 3,3',5,5'-tetramethylbenzidine (TMB) substrate and absorbance was measured at 450nm. For background correction, absorbance values at 550nm were also measured and plotted against ISG15 protein standards. ISG15 protein concentration was then calculated using a linear regression method.

Cytokine quantification

Proinflammatory cytokines and chemokines concentrations were measured by a cytometric beads assay kit (Biolegend Cat#740003), as advised by the manufacturer. Briefly, cytokine/chemokine standards or cleared culture supernatants were mixed with capture beads together with biotin-conjugated antibody cocktail for 2 hours. Phycoerythrin (PE)-conjugated streptavidin was then added to the mixture and incubated for 30 minutes. Beads were pelleted by centrifugation at 3000 x g for 5 minutes, washed, fixed in 4% formaldehyde for 15 minutes, centrifuged at 3,000 x g for 5 minutes, and resuspended in 250µL 1X wash buffer for flow cytometry (BD LSRFortessa) acquisition. Results were analyzed with FCAP array version 3.0 (BD). Specific capture beads groups were first separated by forward scatter (FSC) and side scatter (SSC) dot-plot graphs and further gated by allophycocyanin (APC) fluorescent channel. PE fluorescence read outs were then curve-fitted to a standard curve to estimate the concentration of analytes.

Phagocytosis assay

Macrophages ($1x10^6$) were seeded in 35mm non-cell culture treated polystyrene dish in 500µL RPMI1640 supplemented with 5% autologous plasma, 100U/ml penicillin, and 100µg/ml streptomycin (GIBCO Cat#15140122). Macrophages were infected with the specified strains of influenza virus (MOI = 2) in fresh serum-free medium (GIBCO Cat#12065074). At 24 hours post-infection, $1x10^7$ blue fluorescent latex beads (SpheroTech; 1µm, 10 beads/cells) were added and incubation continued for 1 hour at 37°C. Cells were then detached in 10mM EDTA at 4°C for 20 minutes, centrifuged at 250 x g for 5 minutes at 4°C and eventually fixed in 4% formaldehyde at room temperature for 15 minutes. Macrophages were pelleted at 500 x g for 5 minutes and resuspended in 250µL PBS, pH 7.4, for flow cytometry acquisition as described above.

Drug treatment

Macrophages ($2x10^5$) were seeded in 24-well plates in 500µL RPMI1640-supplemented with 5% autologous plasma, 100U/ml penicillin, and 100µg/ml streptomycin (GIBCO Cat#15140122). Twenty-four hours later, media were discarded and replaced with fresh serum-free medium (GIBCO Cat#12065074), which was

changed daily for 2 days. On the day of experiment, macrophages were pre-treated or post-treated with the indicated drug concentrations as detailed.

LDH assay

LDH-Cytotoxicity Colorimetric Assay Kit II (BioVision Cat#K313) was used to estimate cell death based on the amount of lactate dehydrogenase (LDH) leakage into the cell culture media. Macrophages were cultured as described above; supernatants were collected, cleared by centrifugation at 1,000 x g for 5 minutes, added to 100µL LDH reaction mix in 96-well plates and incubated for 30 minutes at room temperature, followed by absorbance measurement at 450nm. A standard curve was generated from mixing cleared media from detergent treated cells (100% lysis) and untreated cells (0% lysis) at different ratios (8.1, 2.7, 0.9, 0.3, 0.1, 0% lysis) and the obtained results were expressed as percentage of lysis. All measurements were done in duplicates and the average absorbance values from test samples (following subtraction of background signal) were used for calculations.

Protein identification and quantification by Tandem Mass spectrometry

All LC-MS analyses were performed by a ThermoFisher Orbitrap Lumos instrument that was operated in a data dependent acquisition mode to switch between Orbitrap full scan MS and LTQ MS/MS. Mass spectra were analysed by MaxQuant version 1.4.1.2 and the Andromeda search engine. The maximum mass deviation allowed for the monoisotopic precursor ions was 4.5 ppm for monoisotopic precursors and 0.5Da for fragment ions. Trypsin was set as the digestion enzyme with a maximum of two allowed missed cleavages. Cysteine carbamidomethylation was set as a fixed modification, and N-terminal acetylation and methionine oxidation were allowed as variable modifications. The spectra were searched using the Andromeda search engine against the mouse Uniprot sequence database. Protein identification required at least two unique peptides per protein group. The data were filtered for a 1% FDR at the peptide and protein level. We used the Database for Annotation, Visualization and Integrated Discovery to assign Gene Ontology (GO) annotations for cellular component, molecular function and biological process. Principal component analysis (PCA) was performed using the Perseus software version 1.5.0.9 on the proteins common between the cells expressing non-targeting DsiRNA or those targeting ISG15

or Ube1L. Hierarchical clustering analyses were performed using Genesis. Protein expression fold change values were log transformed (base 2). Log transformed fold change data showed bell shaped distributions and were symmetric around 0.

Statistical analysis

Results are shown as mean ± SEM or mean ± sd as indicated, of experiments performed in atleast 3 independent biological replicates. Statistical differences between groups were determined by the Mann-Whitney *U* test, with a confidence limit for significance set at 0.05 or less.

Acknowledgments

We thank the Faculty Core Facility and Centre for Genomic Sciences of the LKS Faculty of Medicine of HKU for providing instruments and technical support; We also acknowledge the support of the clinicians who facilitated this study, including Drs Owen Tak-Yin Tsang, Wai Shing Leung, Jacky Man Chun Chan, Thomas Shiu Hong Chik, Chris Yau Chung Choi, John Yu Hong Chan, Daphne Pui-Lin Lau, and Ying Man Ho as well as the dedicated clinical team at Infectious Diseases Centre, Princess Margaret Hospital, Hospital Authority of Hong Kong; and the patients who kindly consented to participate in this investigation and the Hong Kong Red Cross Blood Transfusion Service for providing buffy coat packs for this research project. We also thank Prof Roberto Bruzzone for comments on the manuscript.

Author Contributions Statement

HHYL, CKPM, and SS designed and conducted the study. HHYL, QT, DM, JH, ES, CKPM, LYLS, WWSN performed and analyzed experiments. HP, BK, AD, AP-F generated critical reagents for the study. JSMP managed the clinical experiments. SS, HHYL and CKPM wrote the manuscript.

Conflict of Interest Statement

The authors declare that the research was conducted in the absence of any commercial or financial relationships that could be construed as a potential conflict of interest.

Funding

This work was supported by research grants from the US National Institute of Allergy and Infectious Diseases (NIAID) under Centers of Excellence for Influenza Research and Surveillance (contract number HHSN272201400006C), the Research Grants Council of the Hong Kong Special Administrative Region (T11-705/14N and 17113019), Health and Medical Research Funds (17161202) and Medical Research Council, UK (MC_PC_19063).

Figure legends

Fig 1. ISG15 and modifying enzymes are induced during virus infections

a-e. Macrophages were infected with the indicated influenza virus strains at a MOI 2. Changes in mRNA expression levels of ISG15 (a) and ISG15 modifying enzymes Ube1L UbcH8, HERC5, USP18 (b-e) against mock infection were quantified by qPCR **f-i.** Macrophages were infected with Zika or SARS-CoV-2 at MOI 2. At indicated time intervals changes in mRNA expression levels of ISG15 (f) and ISG15 modifying enzymes Ube1L UbcH8 and HERC5 (g-i) against mock infection were quantified by qPCR **j, k.** Intracellular ISG15 protein levels in influenza infected cells (j) or Zika or SARS-CoV-2 infected macrophages (k) were quantified by ELISA. Data are displayed as means ± SEM of at least three independent donors. *$p < 0.05$ by the Mann-Whitney U Test vs. mock-infected cells. **l.** ISGylation in virus-infected macrophages was measured for influenza, Zika and SARS-CoV-2. Macrophages were infected with the indicated wild-type and mutated strains of influenza virus *(left panel)*, Zika *(middle panel)* and SARS-CoV-2 *(right panel)* at a MOI 2. Lysates were collected in 1% IGEPAL PBS pH 7.4, separated by SDS-PAGE and visualized by Western blotting using an anti-human ISG15 antibody. Gapdh levels were measured as loading control. The blot is representative of results obtained from three independent donors.

Fig 2. ISG15 is secreted from virus-infected macrophages via non-conventional secretory autophagosomal pathway.

a. Macrophages were infected with the indicated influenza viral strains at a MOI 2. At indicated time intervals changes in extracellular levels of ISG15 were quantified by ELISA. **b, c.** iPSC-derived macrophages were infected with either Zika or SARS-CoV-2 (b) at a MOI 2 or UV-inactivated Zika or SARS-CoV-2 (c). Changes in extracellular levels of ISG15 were quantified by ELISA. **d, e.** Brefeldin (5μM), which inhibits conventional secretion pathway, was added 1 h post-infection and had no effect on ISG15 secretion (d) and protein expression (e) 24 h post infection. **f.** LDH assay was performed using LDH-Cytotoxicity Colorimetric Assay Kit II (BioVision) to estimate cell death based on the amount of LDH leakage into the cell culture media, 24 h post infection following the manufacturer's protocol. **g.** Caspase inhibitors Z-YVAD-FMK and Z-DEVD-FMK were added to virus-infected macrophages (1h post infection), and ISG15 secretion measured 24h post infection. **h, i.** Depletion of proteins implicated in secretory autophagosomes was performed by DsiRNA in iPSC-derived macrophages

and verified by immunoblotting (**Fig S2a, b**). Non-targeting and depleted cells were infected with SARS-CoV-2 (MOI 2; 24h) and secretion of ISG15 measured by ELISA. All data are displayed as means ± SEM of at least three independent donors. *p < 0.05 by the Mann-Whitney U Test vs mock-infected cells.

Fig 3. ISG15 is specifically secreted by monocytic cells during virus infections. **a.** Normal human bronchial epithelial cells (NHBE), macrophages (Mac) and dendritic cells (DCs) were infected with the indicated wild-type and mutated influenza virus strains at a MOI 2. Total RNA was collected at 24 hours post-infection and reverse transcribed into cDNA using oligo-d(T)23VN primer. Relative changes of expression levels against mock infection were quantified by qPCR using gene specific primers. **b.** Quantification of ISG15 copy number was done by RT-qPCR using ISG15 specific primers. **c.** Cell culture media were collected at 24 hours post-infection. ISG15 protein was quantified by ISG15 sandwich ELISA. All data are displayed as mean ± SEM of at least three independent donors. *p < 0.05 by the Mann-Whitney U Test vs. mock-treated cells **d.** NHBE, iPSC-derived macrophages (Mac) and dendritic cells (DCs) were infected with either Zika or SARS-CoV-2 at a MOI 1. Total RNA was collected at 24- and 48-hours post-infection; relative changes of expression levels against mock infection were quantified by qPCR using gene specific primers **e.** Quantification of ISG15 copy number was done by RT-qPCR using ISG15 specific primers **f.** Supernatants from infected cells were collected at 24 and 48 hours post-infection. ISG15 protein was quantified by ISG15 sandwich ELISA. All data are displayed as mean ± sd of at least three independent experiments. *p < 0.05 by the Mann-Whitney U Test vs. mock-treated cells.

Fig 4. Immune dysfunction in SARS-CoV-2-infected macrophages

a. Surface staining of MHC-I in iPSC-derived macrophages infected with SARS-CoV-2 (MOI 2, 24 h). Controls included were antibody isotype, UV-inactivated virus and dsRNA. Cells were gated on viral N+ (in red; 75% of population) and surface MHC-I. Bystander cells are depicted in black. **b.** Surface staining of MHC-II in iPSC-derived macrophages infected with SARS-CoV-2 (MOI 2, 24 h). Cells were gated on viral N+ (in red; 73% of population) and surface MHC-II+ cells. Bystander population is depicted in black. Controls included were antibody isotype, UV-inactivated virus and dsRNA treated cells **c.** iPSC-derived macrophages were stimulated to M1 or M2 by

differentiating for 48 hours in the presence of M-CSF+LPS+IFN-γ and M-CSF+IL-4 respectively, or infected with SARS-CoV-2 (MOI 2, 48h). Expression of key markers of polarization was measured by RT qPCR. **d.** Secretion of indicated cytokines was measured using cytometric bead arrays following the manufacturer's guidelines and flow cytometry. **e.** Quantification of phagocytosis of M1- or M2-stimulated phagocytes was compared with SARS-CoV-2 infected macrophages (MOI 2, 48 h). Error bars represent mean±s.d; [*$p < 0.05$, **$p < 0.01$, ***$p < 0.001$, ****$p < 0.0001$; Two-way ANOVA with Tukey's multiple comparison test].

Fig 5. Role of free versus conjugated ISG15 on viral replication and cytokine secretion.

a. Macrophages were transfected with ISG15, Ube1L, HERC5 or USP18 DsiRNA for 72 hours; depletion was verified in IFN-I treated cells by immunoblotting. **b.** Cellular ISGylation was measured in influenza, Zika and SARS-CoV-2 infected cells (MOI 2), 24 hours post infection **c.** Total RNA was collected at indicated time intervals from influenza, Zika and SARS-CoV-2 infected cells, and reverse transcribed into cDNA using uni-12 primer. Quantifications of absolute copy number were done by RT-qPCR using universal vRNA specific primers. For infectivity assay, culture medium was removed at 6 and 24 hours post-infection from influenza-infected cells and $TCID_{50}$ infectivity assays were done in MDCK cells as described in the Materials and Methods section. $TCID_{50}$/mL value was calculated by the Spearman Kärber method. Data are displayed as means ± SEM of at least three independent donors. There were no statistical differences by the Mann-Whitney U Test vs. control cells treated with non-targeting (NT) DsiRNA **d.** Macrophages were transfected with either non-targeting (NT), ISG15, Ube1L, or USP18 DsiRNA for 72 hours prior to H9N2/Y280 influenza virus infection at MOI 2. Indicated cytokines were quantified by cytometric beads assay. Data are displayed as means ± SEM of at least three independent donors. *p < 0.05 by the Mann-Whitney U Test vs. control **e-f.** iPSC-derived macrophages transfected with either non-targeting (NT), ISG15, Ube1L, HERC5 or USP18 DsiRNA for 72 hours were infected with either Zika (e) or SARS-CoV-2 (f) at MOI 2 for 24 hours. Indicated cytokines were quantified by cytometric beads assay. Data are displayed as means ± s.d of at least three independent experiments. *p < 0.05 by the Mann-Whitney U Test vs. control (NT cells).

Fig 6. Dysregulation of antigen presentation and interferon response in macrophages expressing SARS-CoV-2 PLpro

a, b. Schematic of SARS-CoV-2 PLpro (wild-type and mutant) and their expression in macrophages verified by immunoblotting **c.** Bulk ISGylation in IFN-I treated macrophages expressing either the empty vector, wild-type PLPro, or mutant PLpro in a dose-dependent manner **d, e.** Surface staining of MHC-I in iPSC-derived macrophages expressing either wt HA-PLpro (d) or the catalytic mutant HA-PLpro (C117A) (e) of SARS-CoV-2. Cells were then treated with dsRNA to induce surface expression of MHC-I. For both samples (wt, mutant) >90% of cells stained positive for HA-(PLpro) and dsRNA **f, g.** Same as (d, e) in cells expressing USP18 (wild-type or C64R/C65R mutant). **h.** Secretion of indicated cytokines was measured using cytometric beads assay following the manufacturer's guidelines and flow cytometry. Error bars represent mean±sd from three independent experiments. Data are displayed as means ± s.d. *p < 0.05 by the Mann-Whitney U Test vs. control (empty vector matched cells). **i.** Supernatants from cells described in (h) were collected and ISG15 was quantified by ISG15 sandwich ELISA. All data are displayed as mean ± sd of at least three independent experiments. *p < 0.05 by the Mann-Whitney U Test vs. control cells. **j.** Elevation of ISG15 was found in the plasma samples collected from the COVID-19 patients at their first week of disease onset. *p < 0.05 by the Mann-Whitney U Test vs. healthy donors.

Fig 7. Quantitative analyses of ISG15-dependent responses in SARS-CoV-2 infected macrophages

a. Schematic of the label-free strategy of LC-MS/MS used to study the ISG15-dependent secretome of SARS-CoV-2 infected cells. iPSC-derived macrophages were either transfected with non-targeting DsiRNA or those targeting ISG15 or Ube1L. Conditioned media was collected from control, SARS-CoV-2 infected or IFNγ treated cells. Proteins were extracted from each of the samples, separated by SDS-PAGE and digested with trypsin for LC-MS/MS as described in the Materials and methods **b.** Total numbers of proteins quantified in atleast two biological replicates **c.** Principal component analysis was performed using the Perseus software. Filled squares represent control cells (NT DsiRNA), empty squares ISG15-depleted, filled circles Ube1L-depleted. The uninfected cells are shown in gray and infected cells are shown

in red **d.** The heatmap represents the hierarchical clustering of the common proteins in the secretome for IFNγ treated or SARS-CoV-2 infected cells. The color key represents changes (log2 scale) from dark blue indicating the largest decreases to red indicating the largest increases **e.** Functional annotation of the common proteins identified in all samples was performed by the DAVID software.

References

1. McNab, F., Mayer-Barber, K., Sher, A., Wack, A. & O'Garra, A. Type I interferons in infectious disease. *Nat. Rev. Immunol.* **15**, 87–103 (2015).
2. Schneider, W. M., Chevillotte, M. D. & Rice, C. M. Interferon-stimulated genes: a complex web of host defenses. *Annu. Rev. Immunol.* **32**, 513–545 (2014).
3. Makris, S., Paulsen, M. & Johansson, C. Type I Interferons as Regulators of Lung Inflammation. *Front Immunol* **8**, 259 (2017).
4. García-Sastre, A. Induction and evasion of type I interferon responses by influenza viruses. *Virus Res.* **162**, 12–18 (2011).
5. Taubenberger, J. K. & Morens, D. M. The pathology of influenza virus infections. *Annu Rev Pathol* **3**, 499–522 (2008).
6. Channappanavar, R. & Perlman, S. Pathogenic human coronavirus infections: causes and consequences of cytokine storm and immunopathology. *Semin Immunopathol* **39**, 529–539 (2017).
7. Tay, M. Z., Poh, C. M., Rénia, L., MacAry, P. A. & Ng, L. F. P. The trinity of COVID-19: immunity, inflammation and intervention. *Nature Reviews Immunology* **20**, 363–374 (2020).
8. Davidson, S., Crotta, S., McCabe, T. M. & Wack, A. Pathogenic potential of interferon αβ in acute influenza infection. *Nat Commun* **5**, 3864 (2014).
9. Cheung, C. Y. *et al.* Induction of proinflammatory cytokines in human macrophages by influenza A (H5N1) viruses: a mechanism for the unusual severity of human disease? *Lancet* **360**, 1831–1837 (2002).

10. Zhou, J. *et al.* Differential expression of chemokines and their receptors in adult and neonatal macrophages infected with human or avian influenza viruses. *J. Infect. Dis.* **194**, 61–70 (2006).

11. Oslund, K. L. & Baumgarth, N. Influenza-induced innate immunity: regulators of viral replication, respiratory tract pathology & adaptive immunity. *Future Virol* **6**, 951–962 (2011).

12. McGonagle, D., Sharif, K., O'Regan, A. & Bridgewood, C. The Role of Cytokines including Interleukin-6 in COVID-19 induced Pneumonia and Macrophage Activation Syndrome-Like Disease. *Autoimmun Rev* **19**, 102537 (2020).

13. Short, K. R., Kroeze, E. J. B. V., Fouchier, R. A. M. & Kuiken, T. Pathogenesis of influenza-induced acute respiratory distress syndrome. *Lancet Infect Dis* **14**, 57–69 (2014).

14. Jahan, A. S. *et al.* OTUB1 Is a Key Regulator of RIG-I-Dependent Immune Signaling and Is Targeted for Proteasomal Degradation by Influenza A NS1. *Cell Reports* **30**, 1570-1584.e6 (2020).

15. Zhang, D. & Zhang, D.-E. Interferon-stimulated gene 15 and the protein ISGylation system. *J. Interferon Cytokine Res.* **31**, 119–130 (2011).

16. Giannakopoulos, N. V. *et al.* Proteomic identification of proteins conjugated to ISG15 in mouse and human cells. *Biochem. Biophys. Res. Commun.* **336**, 496–506 (2005).

17. Wong, J. J. Y., Pung, Y. F., Sze, N. S.-K. & Chin, K.-C. HERC5 is an IFN-induced HECT-type E3 protein ligase that mediates type I IFN-induced ISGylation of protein targets. *Proc. Natl. Acad. Sci. U.S.A.* **103**, 10735–10740 (2006).

18. Sanyal, S. *et al.* Type I interferon imposes a TSG101/ISG15 checkpoint at the Golgi for glycoprotein trafficking during influenza virus infection. *Cell Host Microbe* **14**, 510–521 (2013).

19. Morales, D. J. *et al.* Novel mode of ISG15-mediated protection against influenza A virus and Sendai virus in mice. *J. Virol.* **89**, 337–349 (2015).

20. Hsiang, T.-Y., Zhao, C. & Krug, R. M. Interferon-induced ISG15 conjugation inhibits influenza A virus gene expression and replication in human cells. *J. Virol.* **83**, 5971–5977 (2009).

21. Tang, Y. *et al.* HERC5 attenuates influenza A virus by catalyzing ISGylation of viral NS1 protein. *J. Immunol.* **184**, 5777–5790 (2010).

22. Zhao, C., Hsiang, T.-Y., Kuo, R.-L. & Krug, R. M. ISG15 conjugation system targets the viral NS1 protein in influenza A virus-infected cells. *Proc. Natl. Acad. Sci. U.S.A.* **107**, 2253–2258 (2010).

23. Yángüez, E. *et al.* ISG15 regulates peritoneal macrophages functionality against viral infection. *PLoS Pathog.* **9**, e1003632 (2013).

24. Farrell, P. J., Broeze, R. J. & Lengyel, P. Accumulation of an mRNA and protein in interferon-treated Ehrlich ascites tumour cells. *Nature* **279**, 523–525 (1979).

25. Haas, A. L., Ahrens, P., Bright, P. M. & Ankel, H. Interferon induces a 15-kilodalton protein exhibiting marked homology to ubiquitin. *J. Biol. Chem.* **262**, 11315–11323 (1987).

26. Kroeker, A. L., Ezzati, P., Halayko, A. J. & Coombs, K. M. Response of primary human airway epithelial cells to influenza infection: a quantitative proteomic study. *J. Proteome Res.* **11**, 4132–4146 (2012).

27. Radoshevich, L. *et al.* ISG15 counteracts Listeria monocytogenes infection. *Elife* **4**, (2015).

28. Park, J. H. *et al.* Positive feedback regulation of p53 transactivity by DNA damage-induced ISG15 modification. *Nat Commun* **7**, 12513 (2016).

29. Dos Santos, P. F. & Mansur, D. S. Beyond ISGlylation: Functions of Free Intracellular and Extracellular ISG15. *J. Interferon Cytokine Res.* **37**, 246–253 (2017).

30. Hermann, M. & Bogunovic, D. ISG15: In Sickness and in Health. *Trends Immunol.* **38**, 79–93 (2017).

31. Swaim, C. D., Scott, A. F., Canadeo, L. A. & Huibregtse, J. M. Extracellular ISG15 Signals Cytokine Secretion through the LFA-1 Integrin Receptor. *Mol. Cell* **68**, 581-590.e5 (2017).

32. Perng, Y.-C. & Lenschow, D. J. ISG15 in antiviral immunity and beyond. *Nat. Rev. Microbiol.* **16**, 423–439 (2018).

33. Ponpuak, M. *et al.* Secretory autophagy. *Curr. Opin. Cell Biol.* **35**, 106–116 (2015).

805 34. Matrosovich, M. N., Matrosovich, T. Y., Gray, T., Roberts, N. A. & Klenk, H.-D.
806 Human and avian influenza viruses target different cell types in cultures of
807 human airway epithelium. *Proc. Natl. Acad. Sci. U.S.A.* **101**, 4620–4624 (2004).

808 35. Manicassamy, B. *et al.* Analysis of in vivo dynamics of influenza virus infection in
809 mice using a GFP reporter virus. *Proc. Natl. Acad. Sci. U.S.A.* **107**, 11531–11536
810 (2010).

811 36. El Costa, H. *et al.* ZIKA virus reveals broad tissue and cell tropism during the first
812 trimester of pregnancy. *Sci Rep* **6**, 35296 (2016).

813 37. Hui, K. P. Y. *et al.* Tropism, replication competence, and innate immune
814 responses of the coronavirus SARS-CoV-2 in human respiratory tract and
815 conjunctiva: an analysis in ex-vivo and in-vitro cultures. *Lancet Respir Med*
816 (2020) doi:10.1016/S2213-2600(20)30193-4.

817 38. Chen, G. *et al.* Clinical and immunological features of severe and moderate
818 coronavirus disease 2019. *J. Clin. Invest.* **130**, 2620–2629 (2020).

819 39. Channappanavar, R. *et al.* Dysregulated Type I Interferon and Inflammatory
820 Monocyte-Macrophage Responses Cause Lethal Pneumonia in SARS-CoV-
821 Infected Mice. *Cell Host & Microbe* **19**, 181–193 (2016).

822 40. Tate, M. D., Pickett, D. L., van Rooijen, N., Brooks, A. G. & Reading, P. C.
823 Critical role of airway macrophages in modulating disease severity during
824 influenza virus infection of mice. *J. Virol.* **84**, 7569–7580 (2010).

825 41. Yu, W. C. L. *et al.* Viral replication and innate host responses in primary human
826 alveolar epithelial cells and alveolar macrophages infected with influenza H5N1
827 and H1N1 viruses. *J. Virol.* **85**, 6844–6855 (2011).

828 42. Wang, J. *et al.* Innate immune response of human alveolar macrophages during
829 influenza A infection. *PLoS ONE* **7**, e29879 (2012).

830 43. Villarreal, D. O. *et al.* Ubiquitin-like Molecule ISG15 Acts as an Immune Adjuvant
831 to Enhance Antigen-specific CD8 T-cell Tumor Immunity. *Mol. Ther.* **23**, 1653–
832 1662 (2015).

833 44. Fujisawa, H. Inhibitory role of neutrophils on influenza virus multiplication in the
834 lungs of mice. *Microbiol. Immunol.* **45**, 679–688 (2001).

45. Tate, M. D. *et al.* The role of neutrophils during mild and severe influenza virus infections of mice. *PLoS ONE* **6**, e17618 (2011).

46. Camp, J. V. & Jonsson, C. B. A Role for Neutrophils in Viral Respiratory Disease. *Front Immunol* **8**, 550 (2017).

47. Wen, W. *et al.* Immune cell profiling of COVID-19 patients in the recovery stage by single-cell sequencing. *Cell Discov* **6**, 31 (2020).

48. Liu, B. *et al.* Interleukin-18 improves the early defence system against influenza virus infection by augmenting natural killer cell-mediated cytotoxicity. *J. Gen. Virol.* **85**, 423–428 (2004).

49. Wang, Z. *et al.* Recovery from severe H7N9 disease is associated with diverse response mechanisms dominated by $CD8^+$ T cells. *Nat Commun* **6**, 6833 (2015).

50. Padovan, E. *et al.* Interferon stimulated gene 15 constitutively produced by melanoma cells induces e-cadherin expression on human dendritic cells. *Cancer Res.* **62**, 3453–3458 (2002).

51. Bogunovic, D. *et al.* Mycobacterial disease and impaired IFN-γ immunity in humans with inherited ISG15 deficiency. *Science* **337**, 1684–1688 (2012).

52. Rose, C. E., Sung, S.-S. J. & Fu, S. M. Significant involvement of CCL2 (MCP-1) in inflammatory disorders of the lung. *Microcirculation* **10**, 273–288 (2003).

53. Deshmane, S. L., Kremlev, S., Amini, S. & Sawaya, B. E. Monocyte chemoattractant protein-1 (MCP-1): an overview. *J. Interferon Cytokine Res.* **29**, 313–326 (2009).

54. Aldridge, J. R. *et al.* TNF/iNOS-producing dendritic cells are the necessary evil of lethal influenza virus infection. *Proc. Natl. Acad. Sci. U.S.A.* **106**, 5306–5311 (2009).

55. Narasaraju, T., Ng, H. H., Phoon, M. C. & Chow, V. T. K. MCP-1 antibody treatment enhances damage and impedes repair of the alveolar epithelium in influenza pneumonitis. *Am. J. Respir. Cell Mol. Biol.* **42**, 732–743 (2010).

56. Li, W. *et al.* The PB2 mutation with lysine at 627 enhances the pathogenicity of avian influenza (H7N9) virus which belongs to a non-zoonotic lineage. *Sci Rep* **7**, 2352 (2017).

865 57. Mazzoni, A. *et al.* Impaired immune cell cytotoxicity in severe COVID-19 is IL-6
866 dependent. *J. Clin. Invest.* (2020) doi:10.1172/JCI138554.

867 58. Swaim, C. D. *et al.* Modulation of Extracellular ISG15 Signaling by Pathogens
868 and Viral Effector Proteins. *Cell Rep* **31**, 107772 (2020).
869

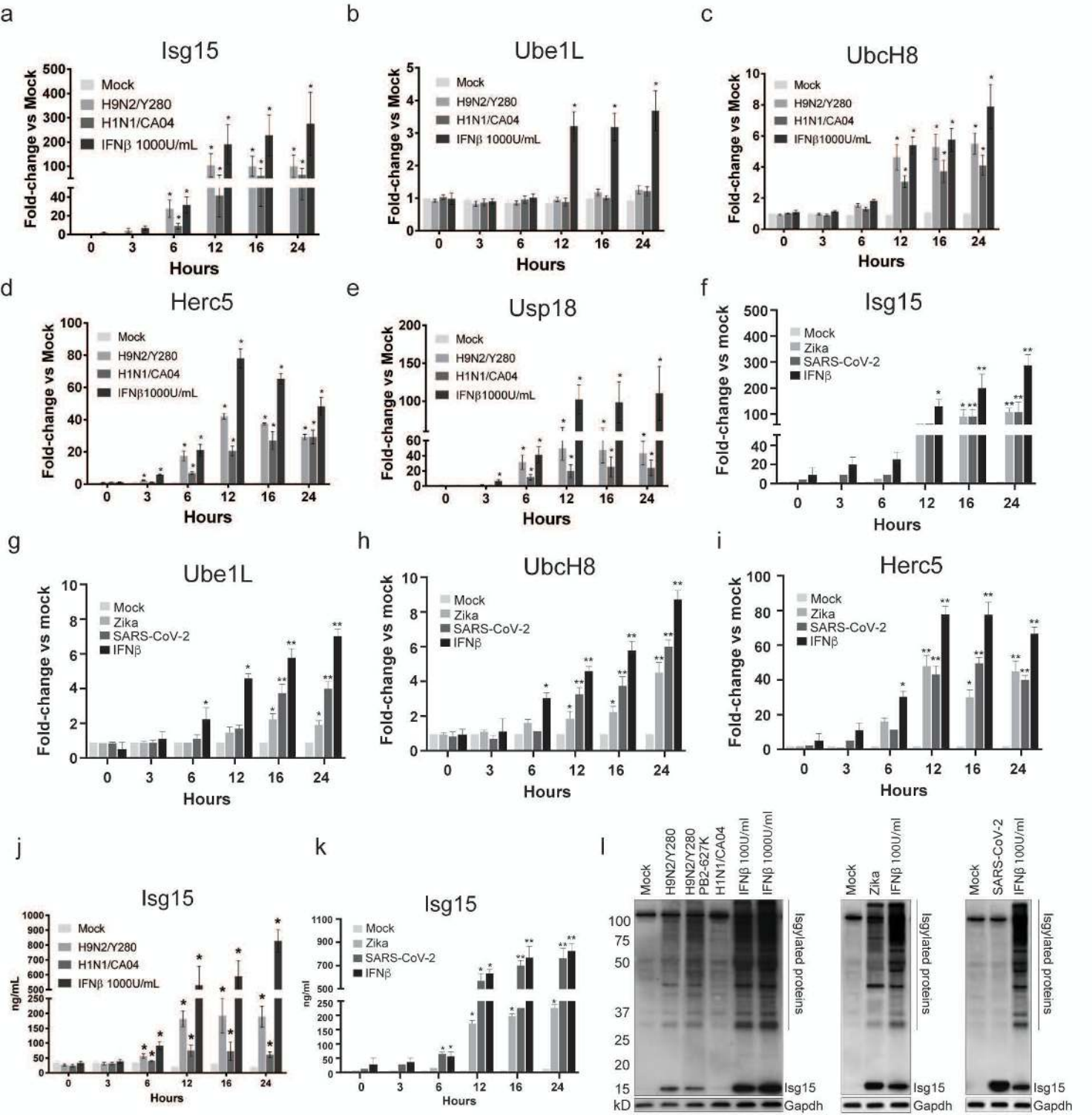
a
Isg15
Fold-change vs Mock
Mock
H9N2/Y280
H1N1/CA04
IFNβ 1000U/mL
Hours
b
Ube1L
Fold-change vs Mock
Mock
H9N2/Y280
H1N1/CA04
IFNβ 1000U/mL
Hours
c
UbcH8
Fold-change vs Mock
Mock
H9N2/Y280
H1N1/CA04
IFNβ1000U/mL
Hours
d
Herc5
Fold-change vs Mock
Mock
H9N2/Y280
H1N1/CA04
IFNβ1000U/mL
Hours
e
Usp18
Fold-change vs Mock
Mock
H9N2/Y280
H1N1/CA04
IFNβ1000U/mL
Hours
f
Isg15
Fold-change vs mock
Mock
Zika
SARS-CoV-2
IFNβ
Hours
g
Ube1L
Fold-change vs mock
Mock
Zika
SARS-CoV-2
IFNβ
Hours
h
UbcH8
Fold-change vs mock
Mock
Zika
SARS-CoV-2
IFNβ
Hours
i
Herc5
Fold-change vs mock
Mock
Zika
SARS-CoV-2
IFNβ
Hours
j
Isg15
ng/mL
Mock
H9N2/Y280
H1N1/CA04
IFNβ 1000U/mL
Hours
k
Isg15
ng/ml
Mock
Zika
SARS-CoV-2
IFNβ
Hours
l
Mock
H9N2/Y280
H9N2/Y280 PB2-627K
H1N1/CA04
IFNβ 100U/ml
IFNβ 1000U/ml
Isgylated proteins
Isg15
Gapdh
kD
Mock
Zika
IFNβ 100U/ml
Isgylated proteins
Isg15
Gapdh
Mock
SARS-CoV-2
IFNβ 100U/ml
Isgylated proteins
Isg15
Gapdh

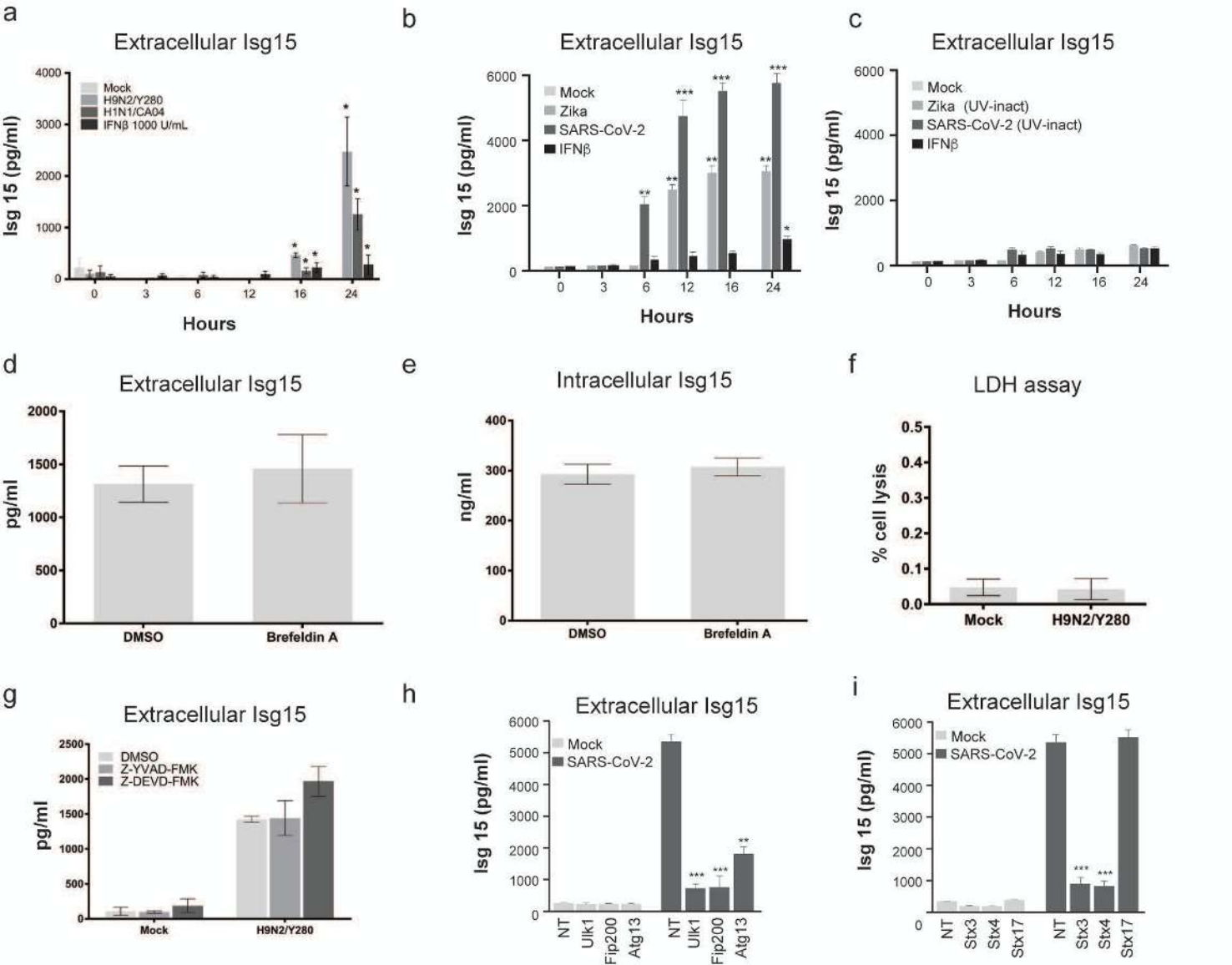
a
Extracellular Isg15
Isg 15 (pg/ml)
Mock
H9N2/Y280
H1N1/CA04
IFNβ 1000 U/mL
Hours
b
Extracellular Isg15
Isg 15 (pg/ml)
Mock
Zika
SARS-CoV-2
IFNβ
Hours
c
Extracellular Isg15
Isg 15 (pg/ml)
Mock
Zika (UV-inact)
SARS-CoV-2 (UV-inact)
IFNβ
Hours
d
Extracellular Isg15
pg/ml
DMSO
Brefeldin A
e
Intracellular Isg15
ng/ml
DMSO
Brefeldin A
f
LDH assay
% cell lysis
Mock
H9N2/Y280
g
Extracellular Isg15
pg/ml
DMSO
Z-YVAD-FMK
Z-DEVD-FMK
Mock
H9N2/Y280
h
Extracellular Isg15
Isg 15 (pg/ml)
Mock
SARS-CoV-2
NT
Ulk1
Fip200
Atg13
i
Extracellular Isg15
Isg 15 (pg/ml)
Mock
SARS-CoV-2
NT
Stx3
Stx4
Stx17

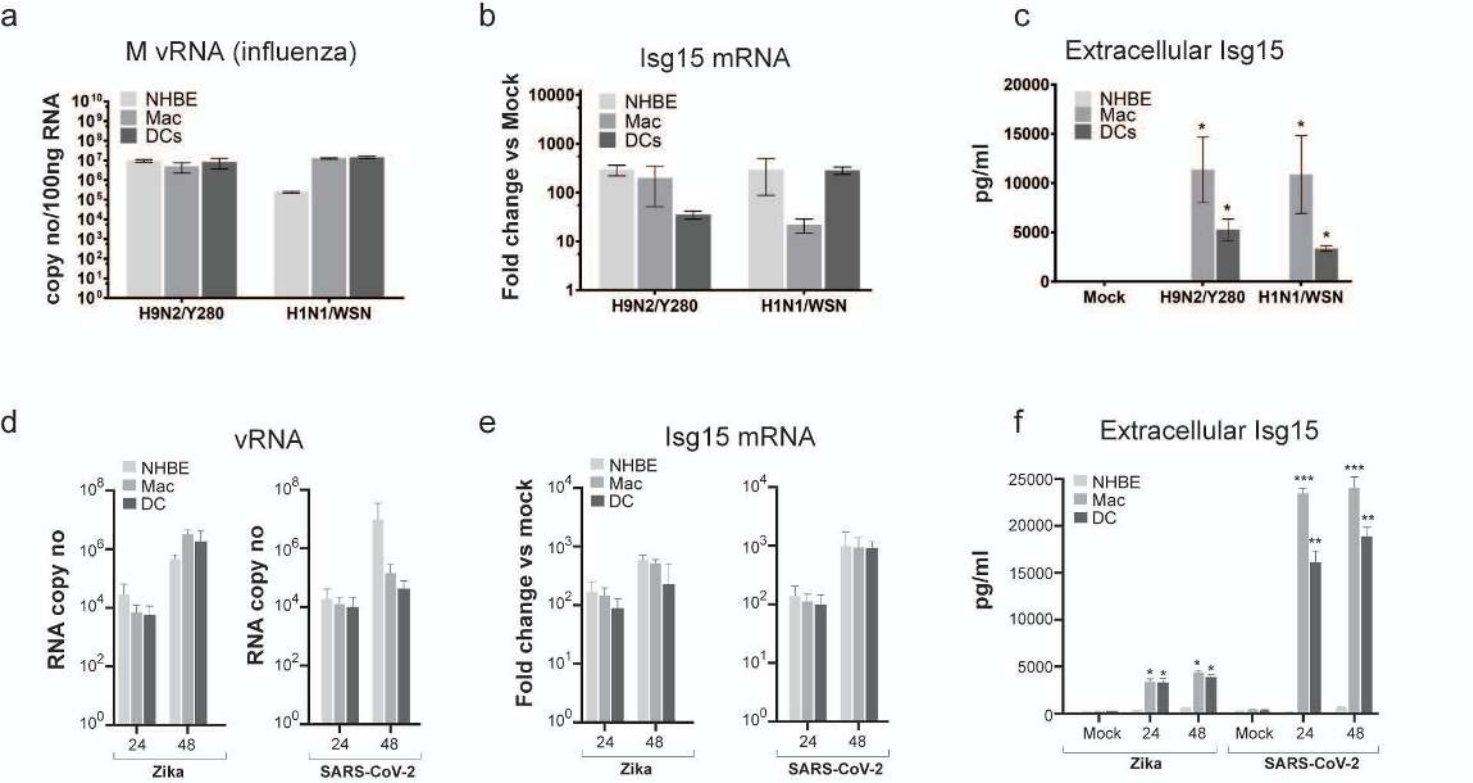
a
M vRNA (influenza)
copy no/100ng RNA
NHBE
Mac
DCs
H9N2/Y280
H1N1/WSN
b
Isg15 mRNA
Fold change vs Mock
NHBE
Mac
DCs
H9N2/Y280
H1N1/WSN
c
Extracellular Isg15
pg/ml
NHBE
Mac
DCs
Mock
H9N2/Y280
H1N1/WSN
d
vRNA
RNA copy no
NHBE
Mac
DC
24
48
Zika
SARS-CoV-2
e
Isg15 mRNA
Fold change vs mock
NHBE
Mac
DC
24
48
Zika
SARS-CoV-2
f
Extracellular Isg15
pg/ml
NHBE
Mac
DC
Mock
24
48
Zika
SARS-CoV-2

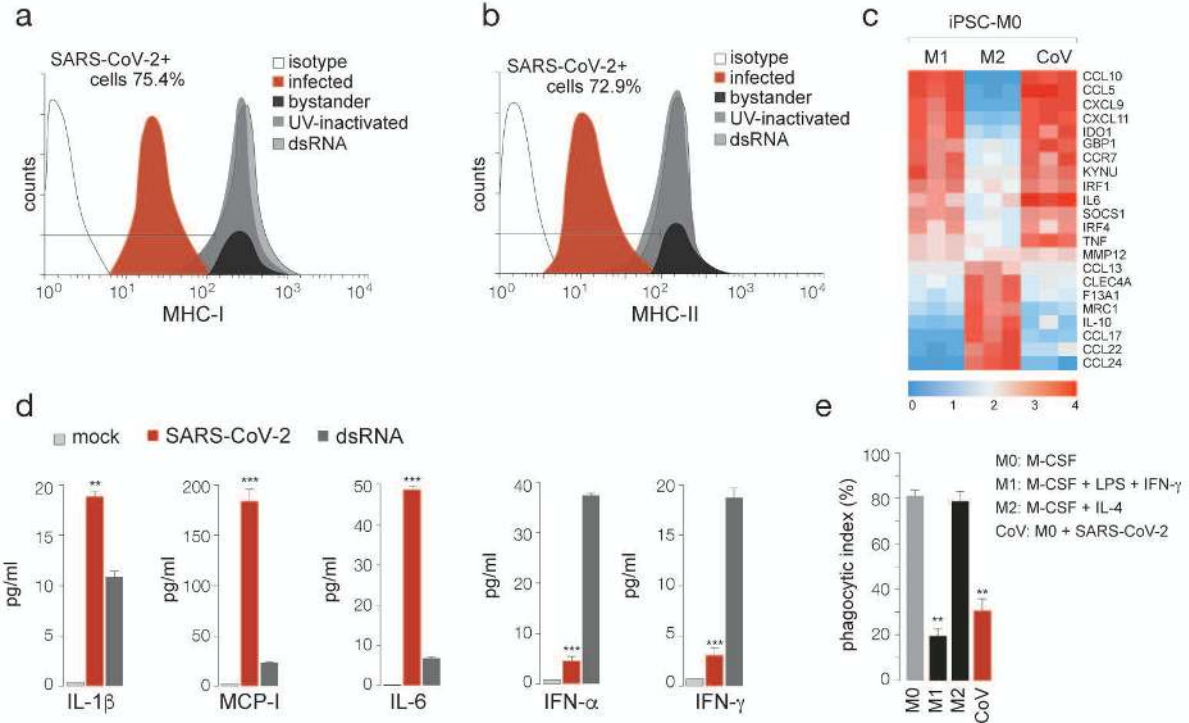
a
SARS-CoV-2+
cells 75.4%
isotype
infected
bystander
UV-inactivated
dsRNA
counts
MHC-I
b
SARS-CoV-2+
cells 72.9%
MHC-II
c
iPSC-M0
M1
M2
CoV
CCL10
CCL5
CXCL9
CXCL11
IDO1
GBP1
CCR7
KYNU
IRF1
IL6
SOCS1
IRF4
TNF
MMP12
CCL13
CLEC4A
F13A1
MRC1
IL-10
CCL17
CCL22
CCL24
d
mock
SARS-CoV-2
dsRNA
pg/ml
IL-1β
MCP-I
IL-6
IFN-α
IFN-γ
e
phagocytic index (%)
M0: M-CSF
M1: M-CSF + LPS + IFN-γ
M2: M-CSF + IL-4
CoV: M0 + SARS-CoV-2
M0
M1
M2
CoV

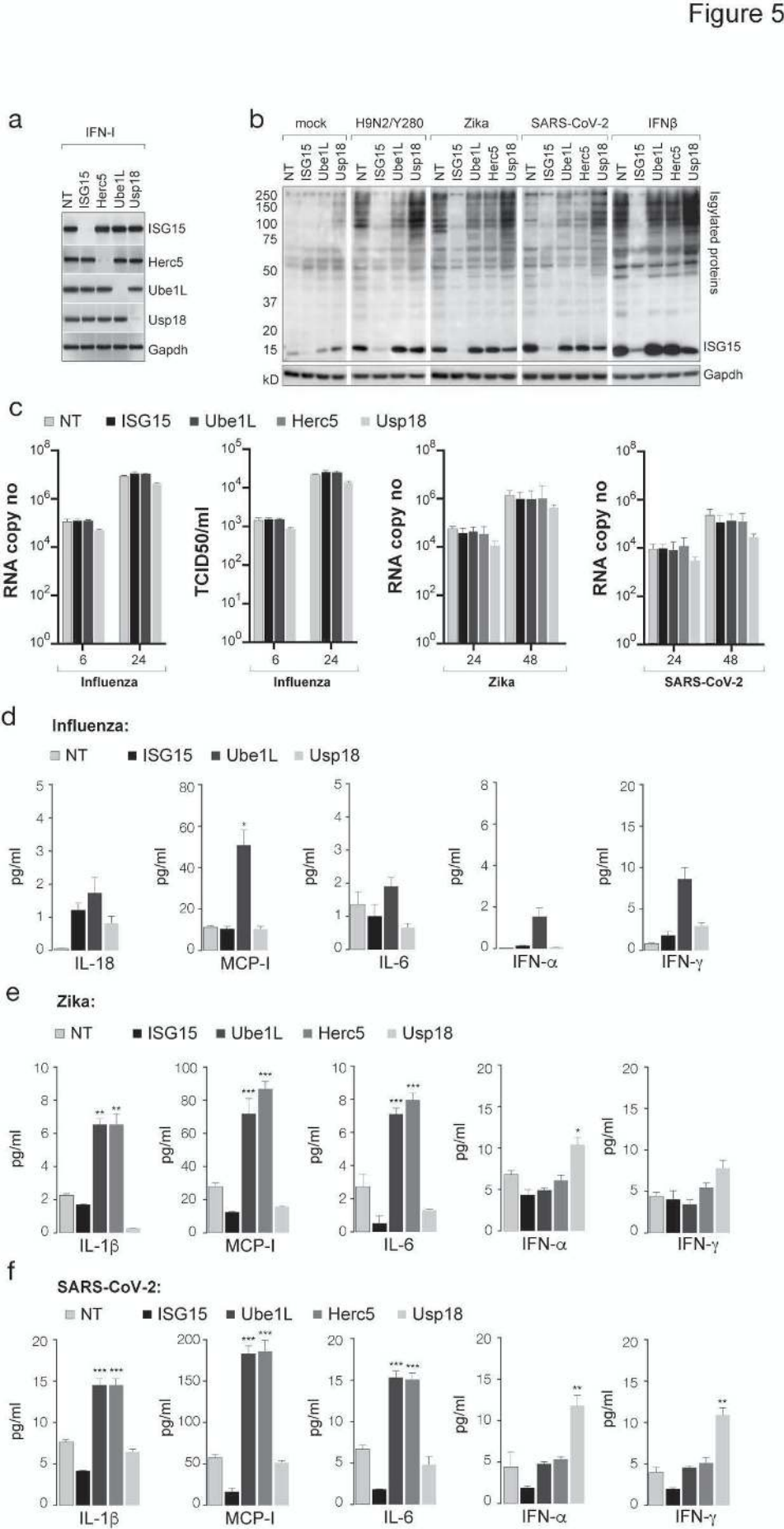
a
IFN-I
NT
ISG15
Herc5
Ube1L
Usp18
ISG15
Herc5
Ube1L
Usp18
Gapdh
b
mock
H9N2/Y280
Zika
SARS-CoV-2
IFNβ
NT
ISG15
Ube1L
Herc5
Usp18
250
150
100
75
50
37
20
15
kD
Isg15ylated proteins
ISG15
Gapdh
c
NT
ISG15
Ube1L
Herc5
Usp18
RNA copy no
TCID50/ml
RNA copy no
RNA copy no
6
24
Influenza
6
24
Influenza
24
48
Zika
24
48
SARS-CoV-2
d
Influenza:
NT
ISG15
Ube1L
Usp18
pg/ml
IL-18
MCP-I
IL-6
IFN-α
IFN-γ
e
Zika:
NT
ISG15
Ube1L
Herc5
Usp18
pg/ml
IL-1β
MCP-I
IL-6
IFN-α
IFN-γ
f
SARS-CoV-2:
NT
ISG15
Ube1L
Herc5
Usp18
pg/ml
IL-1β
MCP-I
IL-6
IFN-α
IFN-γ

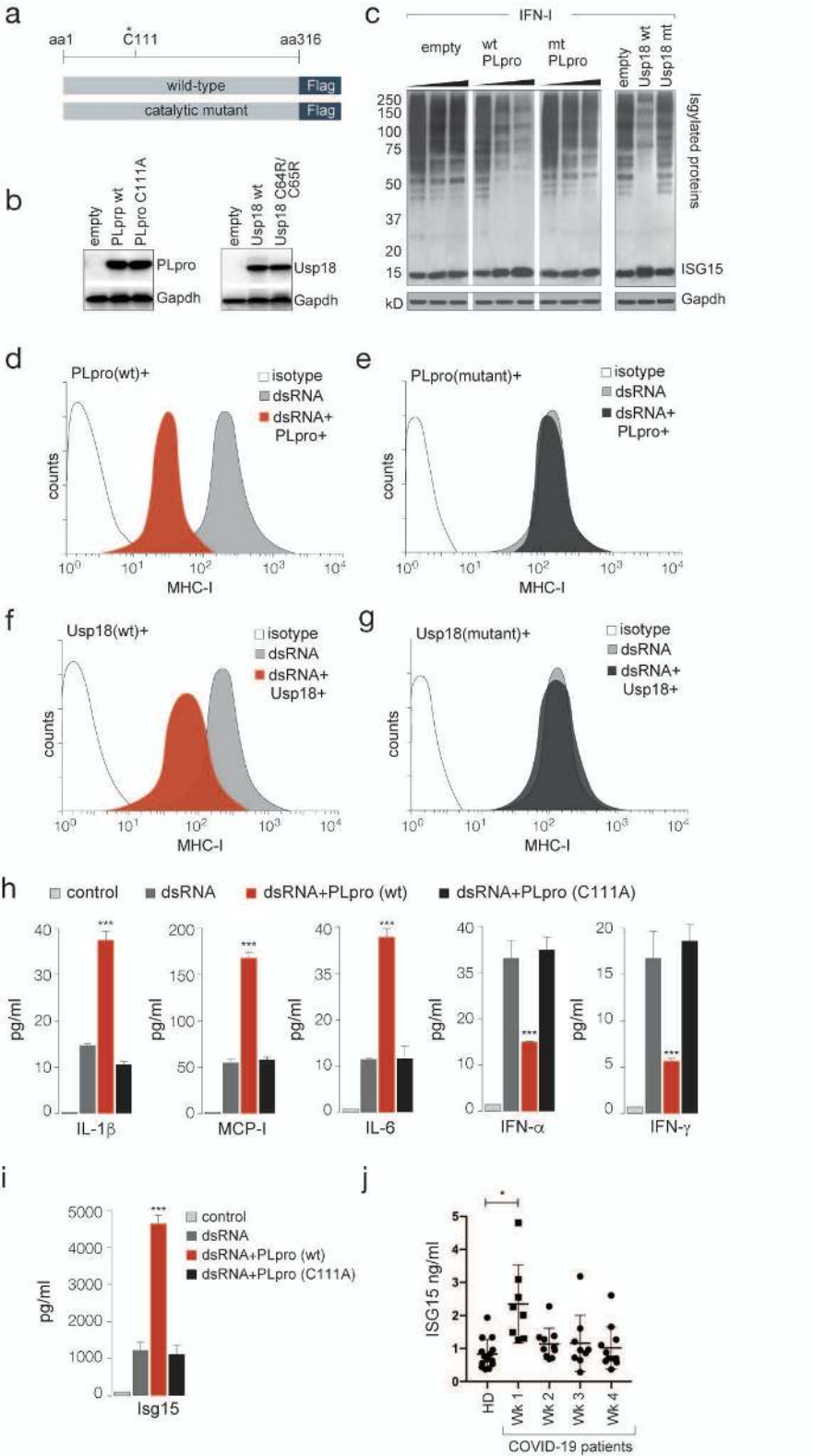
a
aa1
C111
aa316
wild-type
Flag
catalytic mutant
Flag
b
empty
PLprp wt
PLpro C111A
PLpro
Gapdh
empty
Usp18 wt
Usp18 C64R/ C65R
Usp18
Gapdh
c
IFN-I
empty
wt PLpro
mt PLpro
empty
Usp18 wt
Usp18 mt
250
150
100
75
50
37
20
15
kD
Isgylated proteins
ISG15
Gapdh
d
PLpro(wt)+
isotype
dsRNA
dsRNA+ PLpro+
counts
MHC-I
e
PLpro(mutant)+
isotype
dsRNA
dsRNA+ PLpro+
counts
MHC-I
f
Usp18(wt)+
isotype
dsRNA
dsRNA+ Usp18+
counts
MHC-I
g
Usp18(mutant)+
isotype
dsRNA
dsRNA+ Usp18+
counts
MHC-I
h
control
dsRNA
dsRNA+PLpro (wt)
dsRNA+PLpro (C111A)
pg/ml
IL-1β
MCP-I
IL-6
IFN-α
IFN-γ
i
control
dsRNA
dsRNA+PLpro (wt)
dsRNA+PLpro (C111A)
pg/ml
Isg15
j
ISG15 ng/ml
HD
Wk 1
Wk 2
Wk 3
Wk 4
COVID-19 patients

Figure 7

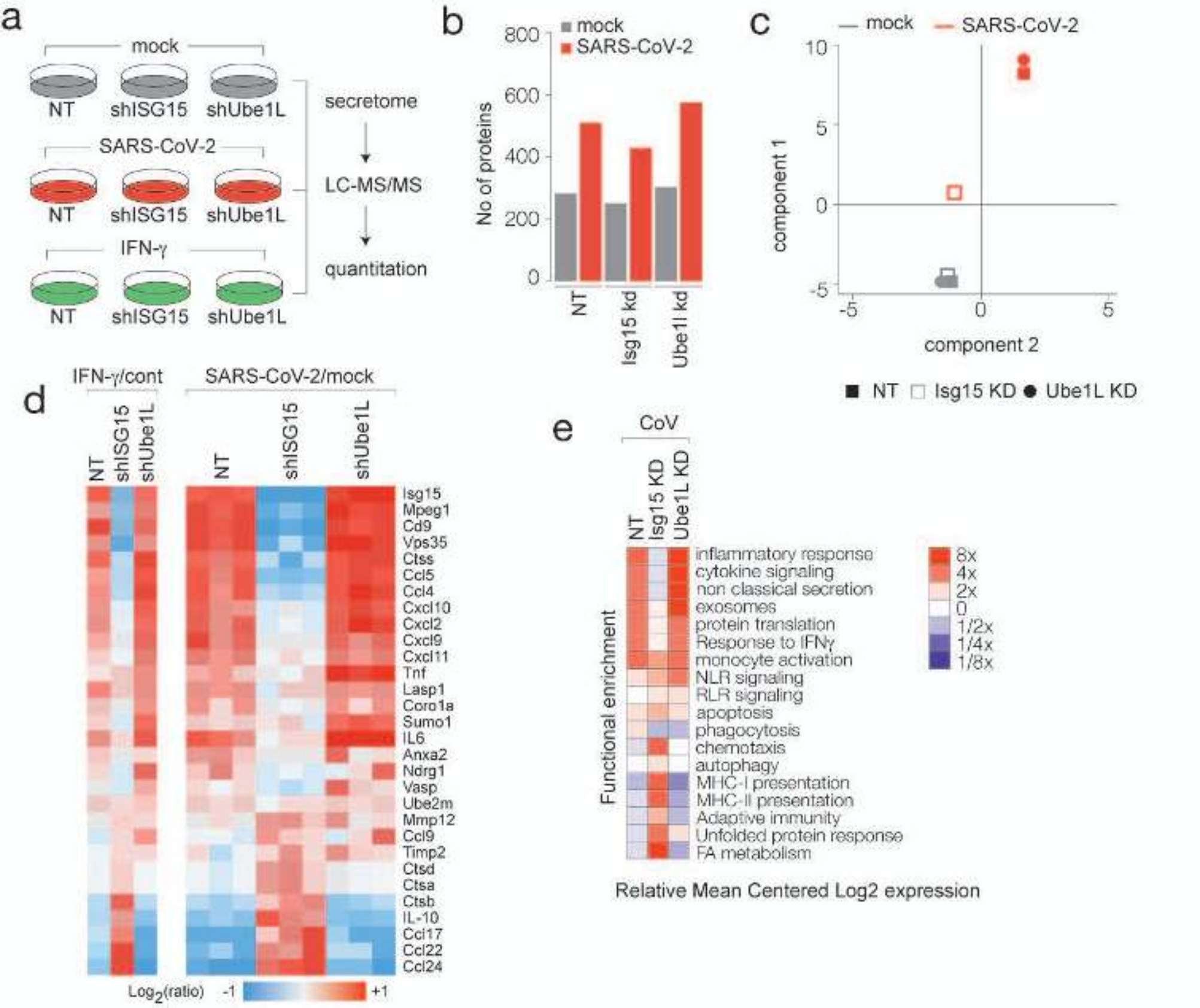
a
mock
NT
shISG15
shUbe1L
SARS-CoV-2
NT
shISG15
shUbe1L
IFN-γ
NT
shISG15
shUbe1L
secretome
LC-MS/MS
quantitation
b
mock
SARS-CoV-2
No of proteins
800
600
400
200
0
NT
Isg15 kd
Ube1l kd
c
mock
SARS-CoV-2
component 1
component 2
10
5
0
-5
-5
0
5
NT
Isg15 KD
Ube1L KD
d
IFN-γ/cont
SARS-CoV-2/mock
NT
shISG15
shUbe1L
NT
shISG15
shUbe1L
Isg15
Mpeg1
Cd9
Vps35
Ctss
Ccl5
Ccl4
Cxcl10
Cxcl2
Cxcl9
Cxcl11
Tnf
Lasp1
Coro1a
Sumo1
IL6
Anxa2
Ndrg1
Vasp
Ube2m
Mmp12
Ccl9
Timp2
Ctsd
Ctsa
Ctsb
IL-10
Cci17
Ccl22
Ccl24
Log2(ratio)
-1
+1
e
CoV
NT
Isg15 KD
Ube1L KD
Functional enrichment
inflammatory response
cytokine signaling
non classical secretion
exosomes
protein translation
Response to IFNγ
monocyte activation
NLR signaling
RLR signaling
apoptosis
phagocytosis
chemotaxis
autophagy
MHC-I presentation
MHC-II presentation
Adaptive immunity
Unfolded protein response
FA metabolism
8x
4x
2x
0
1/2x
1/4x
1/8x
Relative Mean Centered Log2 expression

Figures

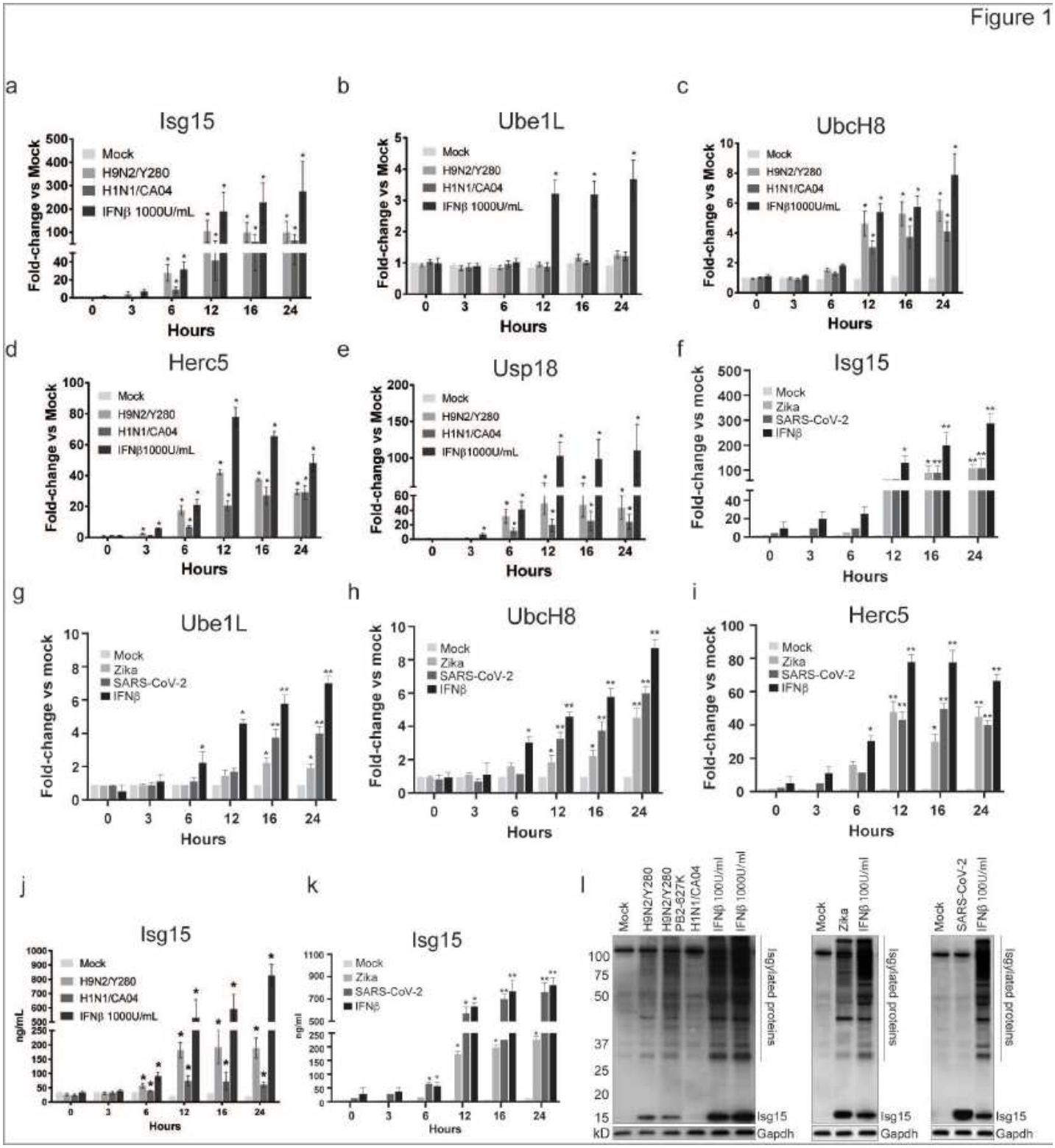

Figure 1

ISG15 and modifying enzymes are induced during virus infections a-e. Macrophages were infected with the indicated influenza virus strains at a MOI 2. Changes in mRNA expression levels of ISG15 (a) and ISG15 modifying enzymes Ube1L UbcH8, HERC5, USP18 (b-e) against mock infection were quantified by

qPCR f-i. Macrophages were infected with Zika or SARS-CoV-2 at MOI 2. At indicated time intervals changes in mRNA expression levels of ISG15 (f) and ISG15 modifying enzymes Ube1L UbcH8 and HERC5 (g-i) against mock infection were quantified by qPCR j, k. Intracellular ISG15 protein levels in influenza infected cells (j) or Zika or SARS-CoV-2 infected macrophages (k) were quantified by ELISA. Data are displayed as means ± SEM of at least three independent donors. *p < 0.05 by the Mann-Whitney U Test vs. mock-infected cells. l. ISGylation in virus-infected macrophages was measured for influenza, Zika and SARS-CoV-2. Macrophages were infected with the indicated wild-type and mutated strains of influenza virus (left panel), Zika (middle panel) and SARS-CoV-2 (right panel) at a MOI 2. Lysates were collected in 1% IGEPAL PBS pH 7.4, separated by SDS-PAGE and visualized by Western blotting using an anti-human ISG15 antibody. Gapdh levels were measured as loading control. The blot is representative of results obtained from three independent donors.

Figure 2

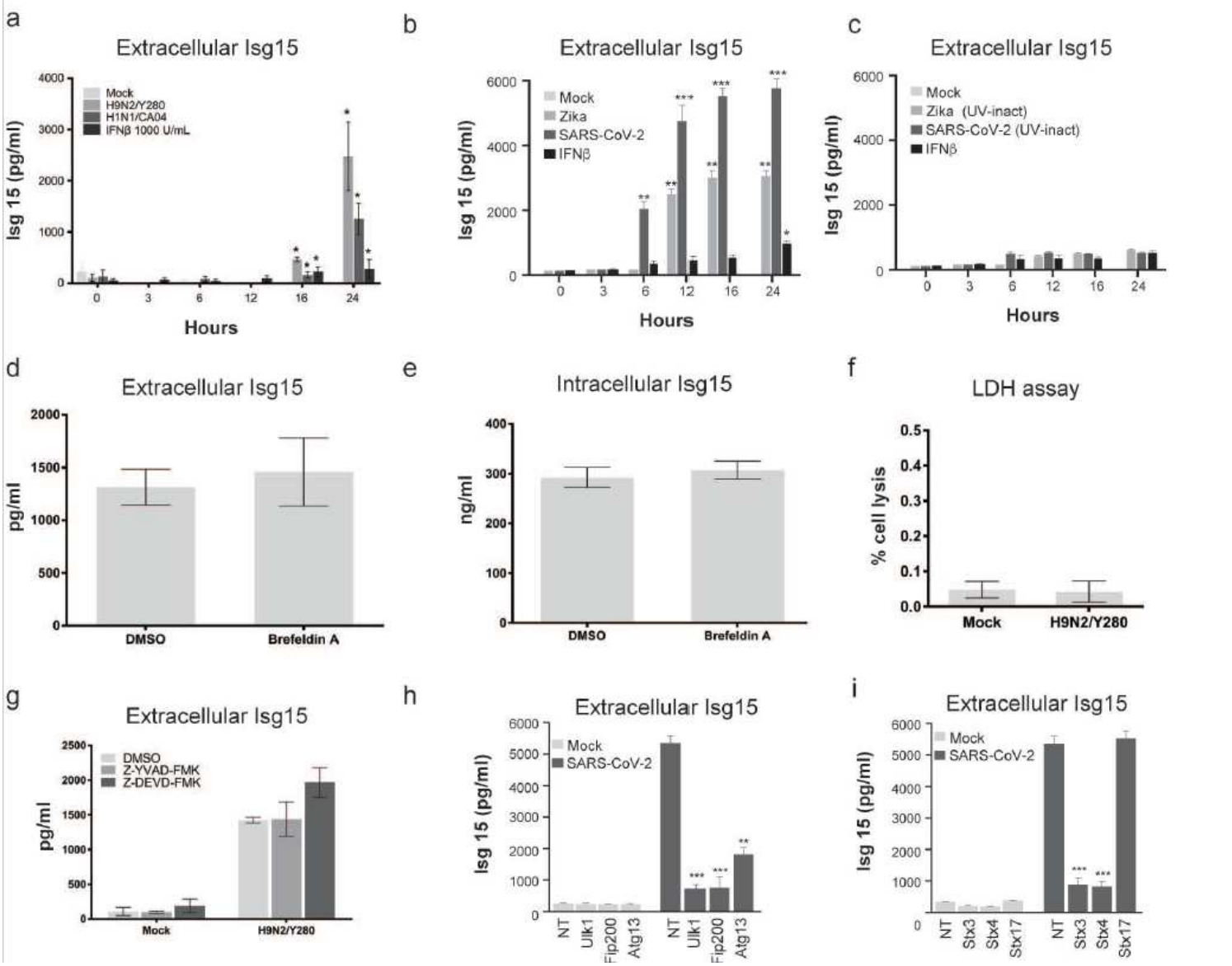

Figure 2

ISG15 is secreted from virus-infected macrophages via non-conventional secretory autophagosomal pathway. a. Macrophages were infected with the indicated influenza viral strains at a MOI 2. At indicated time intervals changes in extracellular levels of ISG15 were quantified by ELISA. b, c. iPSC-derived macrophages were infected with either Zika or SARS-CoV- 2 (b) at a MOI 2 or UV-inactivated Zika or SARS-CoV-2 (c). Changes in extracellular levels of ISG15 were quantified by ELISA. d, e. Brefeldin (5μM), which inhibits conventional secretion pathway, was added 1 h post-infection and had no effect on ISG15 secretion (d) and protein expression (e) 24 h post infection. f. LDH assay was performed using LDH-Cytotoxicity Colorimetric Assay Kit II (BioVision) to estimate cell death based on the amount of LDH leakage into the cell culture media, 24 h post infection following the manufacturer's protocol. g. Caspase inhibitors Z-YVAD-FMK and Z-DEVD-FMK were added to virus-infected macrophages (1h post infection), and ISG15 secretion measured 24h post infection. h, i. Depletion of proteins implicated in secretory autophagosomes was performed by DsiRNA in iPSC-derived macrophages and verified by immunoblotting (Fig S2a, b). Non-targeting and depleted cells were infected with SARS-CoV-2 (MOI 2; 24h) and secretion of ISG15 measured by ELISA. All data are displayed as means ± SEM of at least three independent donors. *p < 0.05 by the Mann-Whitney U Test vs mock-infected cells.

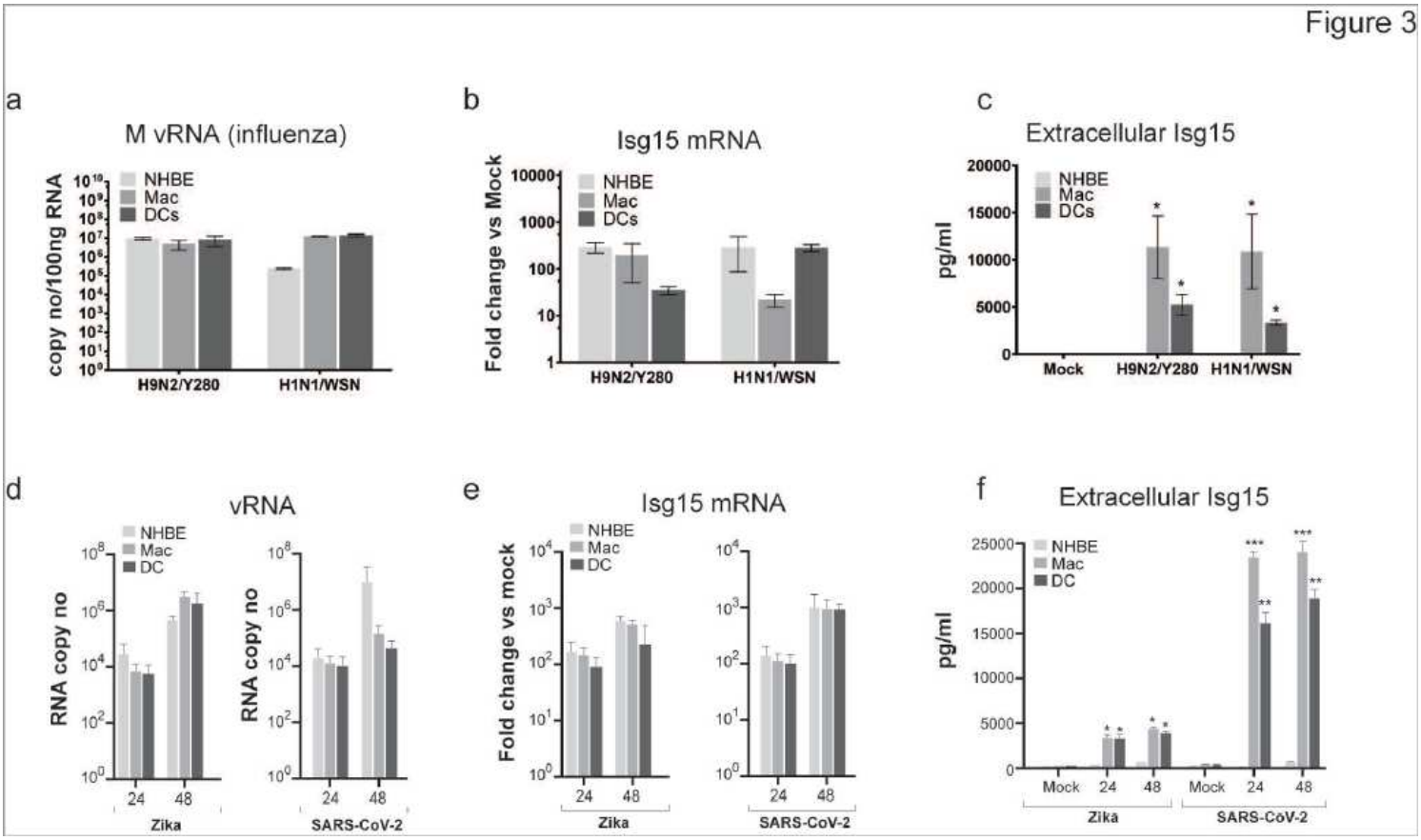

Figure 3

ISG15 is specifically secreted by monocytic cells during virus infections. a. Normal human bronchial epithelial cells (NHBE), macrophages (Mac) and dendritic cells (DCs) were infected with the indicated wild-type and mutated influenza virus strains at a MOI 2. Total RNA was collected at 24 hours post-infection and reverse transcribed into cDNA using oligo-d(T)23VN primer. Relative changes of expression

levels against mock infection were quantified by qPCR using gene specific primers. b. Quantification of ISG15 copy number was done by RT-qPCR using ISG15 specific primers. c. Cell culture media were collected at 24 hours post-infection. ISG15 protein was quantified by ISG15 sandwich ELISA. All data are displayed as mean ± SEM of at least three independent donors. *p < 0.05 by the Mann-Whitney U Test vs. mock treated cells d. NHBE, iPSC-derived macrophages (Mac) and dendritic cells (DCs) were infected with either Zika or SARS-CoV-2 at a MOI 1. Total RNA was collected at 24- and 48-hours post-infection; relative changes of expression levels against mock infection were quantified by qPCR using gene specific primers e. Quantification of ISG15 copy number was done by RT-qPCR using ISG15 specific primers f. Supernatants from infected cells were collected at 24 and 48 hours post-infection. ISG15 protein was quantified by ISG15 sandwich ELISA. All data are displayed as mean ± sd of at least three independent experiments. *p < 0.05 by the Mann-Whitney U Test vs. mock-treated cells.

Figure 4

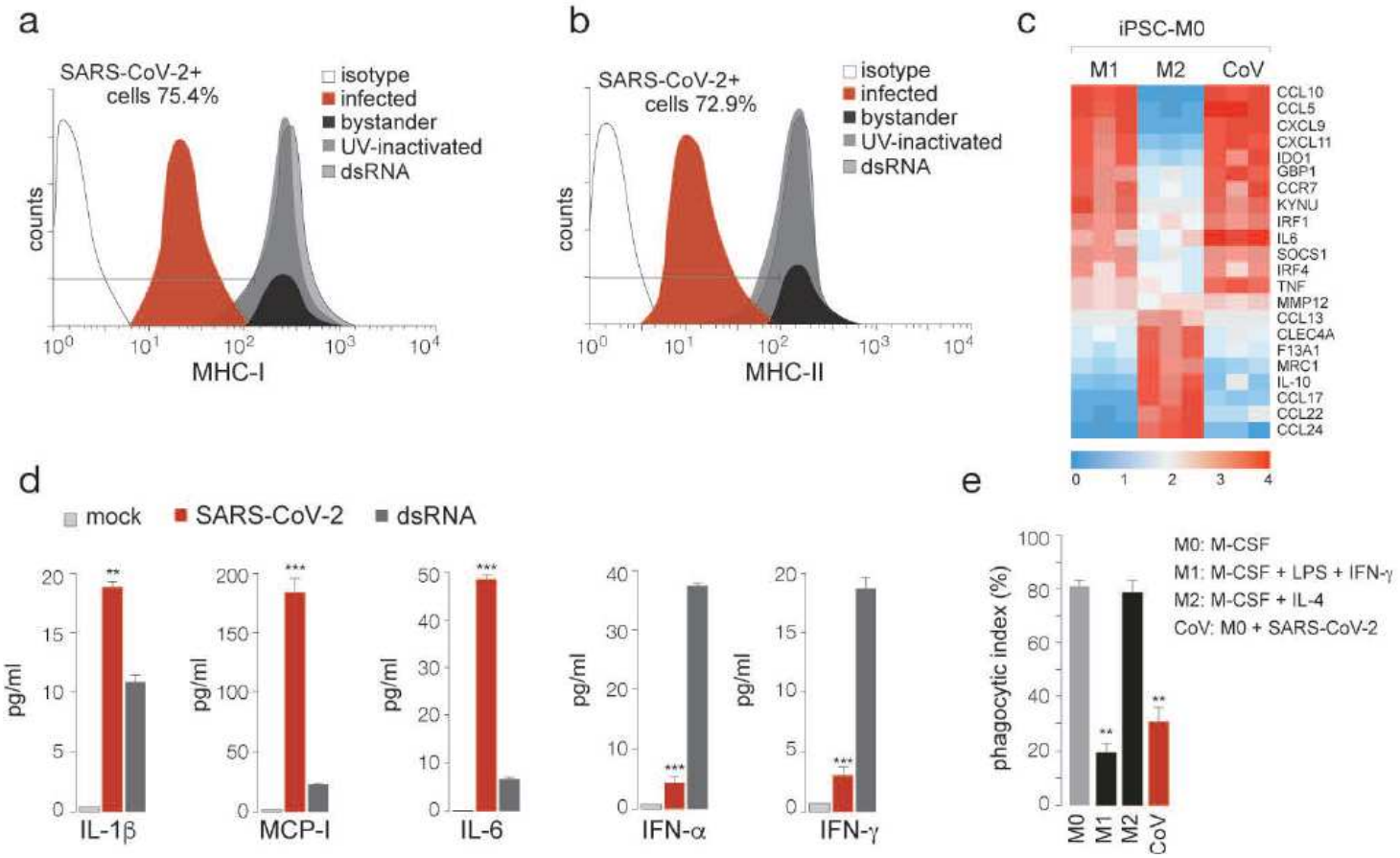

Figure 4

Immune dysfunction in SARS-CoV-2-infected macrophages a. Surface staining of MHC-I in iPSC-derived macrophages infected with SARS-CoV- 2 (MOI 2, 24 h). Controls included were antibody isotype, UV-inactivated virus and dsRNA. Cells were gated on viral N+ (in red; 75% of population) and surface MHC-I. Bystander cells are depicted in black. b. Surface staining of MHC-II in iPSC-derived macrophages infected

with SARS-CoV-2 (MOI 2, 24 h). Cells were gated on viral N+ (in red; 73% of population) and surface MHC-II+ cells. Bystander population is depicted in black. Controls included were antibody isotype, UV-inactivated virus and dsRNA treated cells c. iPSC-derived macrophages were stimulated to M1 or M2 by differentiating for 48 hours in the presence of M-CSF+LPS+IFN-g and M-CSF+IL-4 respectively, or infected with SARS-CoV-2 (MOI 2, 48h). Expression of key markers of polarization was measured by RT qPCR. d. Secretion of indicated cytokines was measured using cytometric bead arrays following the manufacturer's guidelines and flow cytometry. e. Quantification of phagocytosis of M1- or M2-stimulated phagocytes was compared with SARS-CoV-2 infected macrophages (MOI 2, 48 h). Error bars represent mean±s.d; [*$p < 0.05$, **$p < 0.01$, ***$p < 0.001$, ****$p < 0.0001$; Two-way ANOVA with Tukey's multiple comparison test].

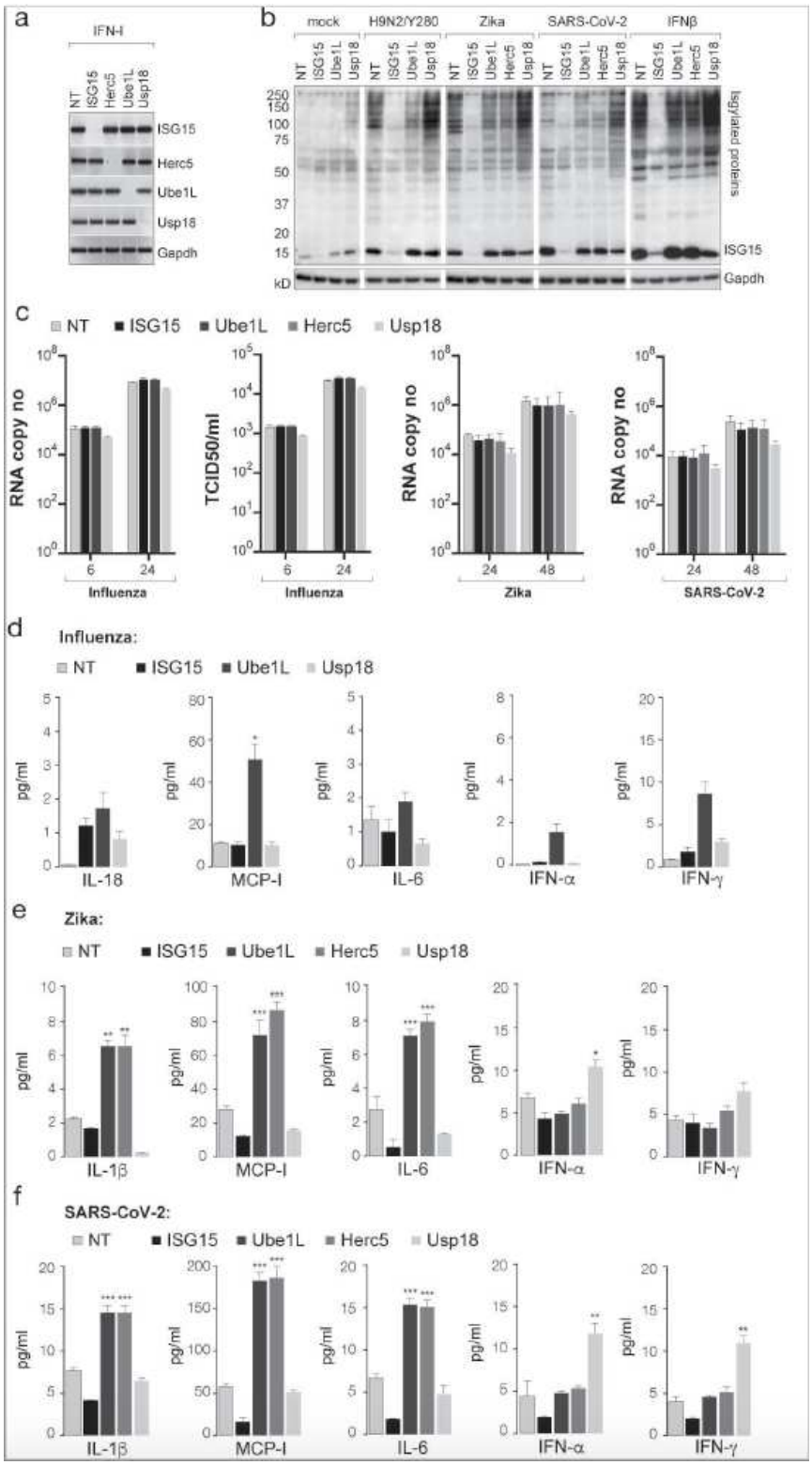

Figure 5

Role of free versus conjugated ISG15 on viral replication and cytokine secretion. a. Macrophages were transfected with ISG15, Ube1L, HERC5 or USP18 DsiRNA for 72 hours; depletion was verified in IFN-I treated cells by immunoblotting. b. Cellular ISGylation was measured in influenza, Zika and SARS-CoV-2 infected cells (MOI 2), 24 hours post infection c. Total RNA was collected at indicated time intervals from influenza, Zika and SARS-CoV-2 infected cells, and reverse transcribed into cDNA using uni-12 primer.

Quantifications of absolute copy number were done by RT-qPCR using universal vRNA specific primers. For infectivity assay, culture medium was removed at 6 and 24 hours post-infection from influenza-infected cells and TCID50 infectivity assays were done in MDCK cells as described in the Materials and Methods section. TCID50/mL value was calculated by the Spearman Kärber method. Data are displayed as means ± SEM of at least three independent donors. There were no statistical differences by the Mann-Whitney U Test vs. control cells treated with non targeting (NT) DsiRNA d. Macrophages were transfected with either non-targeting (NT), ISG15, Ube1L, or USP18 DsiRNA for 72 hours prior to H9N2/Y280 influenza virus infection at MOI 2. Indicated cytokines were quantified by cytometric beads assay. Data are displayed as means ± SEM of at least three independent donors. *p < 0.05 by the Mann-Whitney U Test vs. control e-f. iPSC-derived macrophages transfected with either non-targeting (NT), ISG15, Ube1L, HERC5 or USP18 DsiRNA for 72 hours were infected with either Zika (e) or SARS-CoV-2 (f) at MOI 2 for 24 hours. Indicated cytokines were quantified by cytometric beads assay. Data are displayed as means ± s.d of at least three independent experiments. *p < 0.05 by the Mann-Whitney U Test vs. control (NT cells).

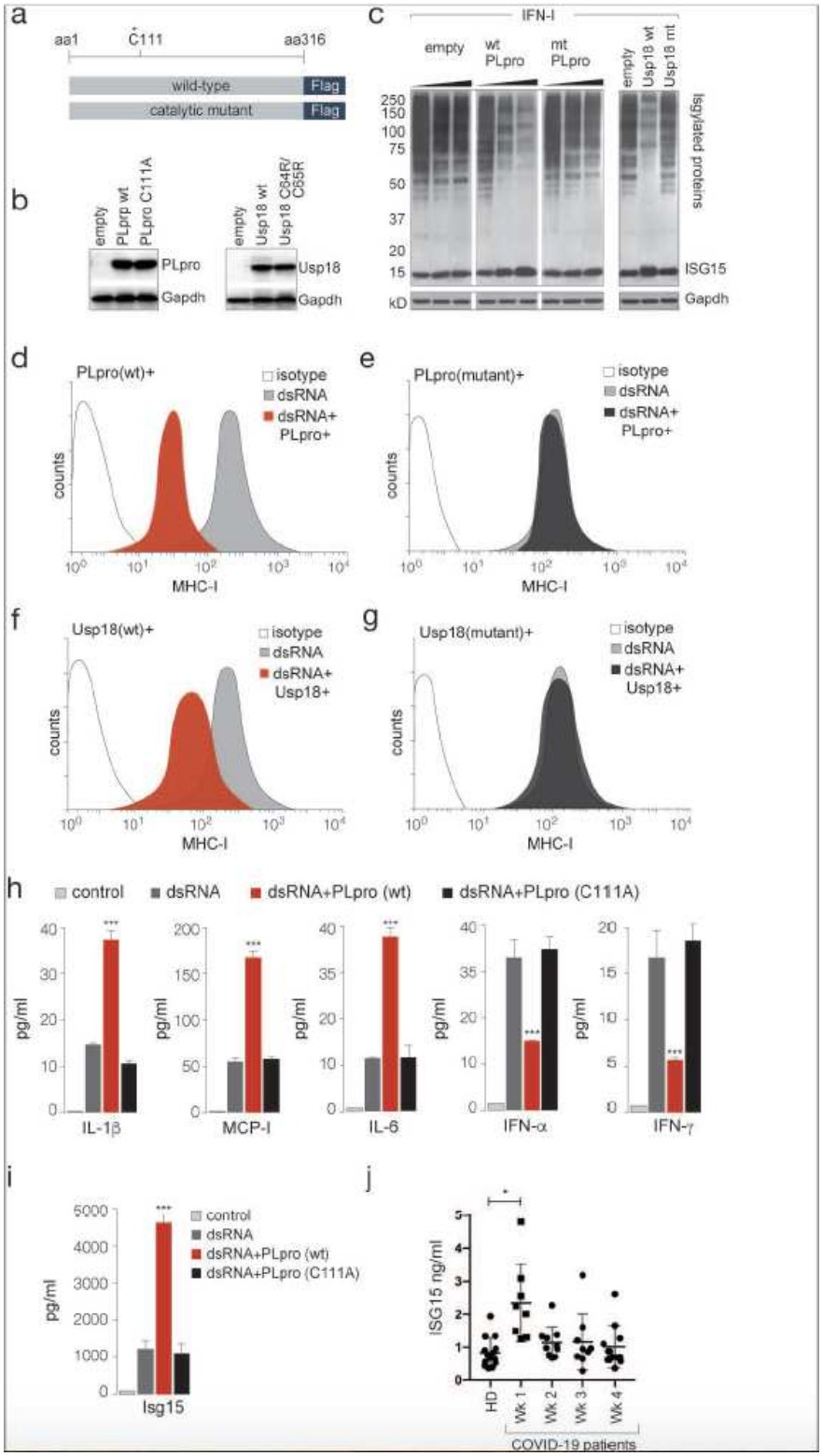

Figure 6

Dysregulation of antigen presentation and interferon response in macrophages expressing SARS-CoV-2 PLpro a, b. Schematic of SARS-CoV-2 PLpro (wild-type and mutant) and their expression in macrophages verified by immunoblotting c. Bulk ISGylation in IFN-I treated macrophages expressing either the empty vector, wild-type PLPro, or mutant PLpro in a dose-dependent manner d, e. Surface staining of MHC-I in iPSC-derived macrophages expressing either wt HA-PLpro (d) or the catalytic mutant HA-PLpro (C117A)

(e) of SARS-CoV-2. Cells were then treated with dsRNA to induce surface expression of MHC-I. For both samples (wt, mutant) >90% of cells stained positive for HA-(PLpro) and dsRNA f, g. Same as (d, e) in cells expressing USP18 (wild-type or C64R/C65R mutant). h. Secretion of indicated cytokines was measured using cytometric beads assay following the manufacturer's guidelines and flow cytometry. Error bars represent mean±sd from three independent experiments. Data are displayed as means ± s.d. *p < 0.05 by the Mann-Whitney U Test vs. control (empty vector matched cells). i. Supernatants from cells described in (h) were collected and ISG15 was quantified by ISG15 sandwich ELISA. All data are displayed as mean ± sd of at least three independent experiments. *p < 0.05 by the Mann-Whitney U Test vs. control cells. j. Elevation of ISG15 was found in the plasma samples collected from the COVID-19 patients at their first week of disease onset. *p < 0.05 by the Mann-Whitney U Test vs. healthy donors.

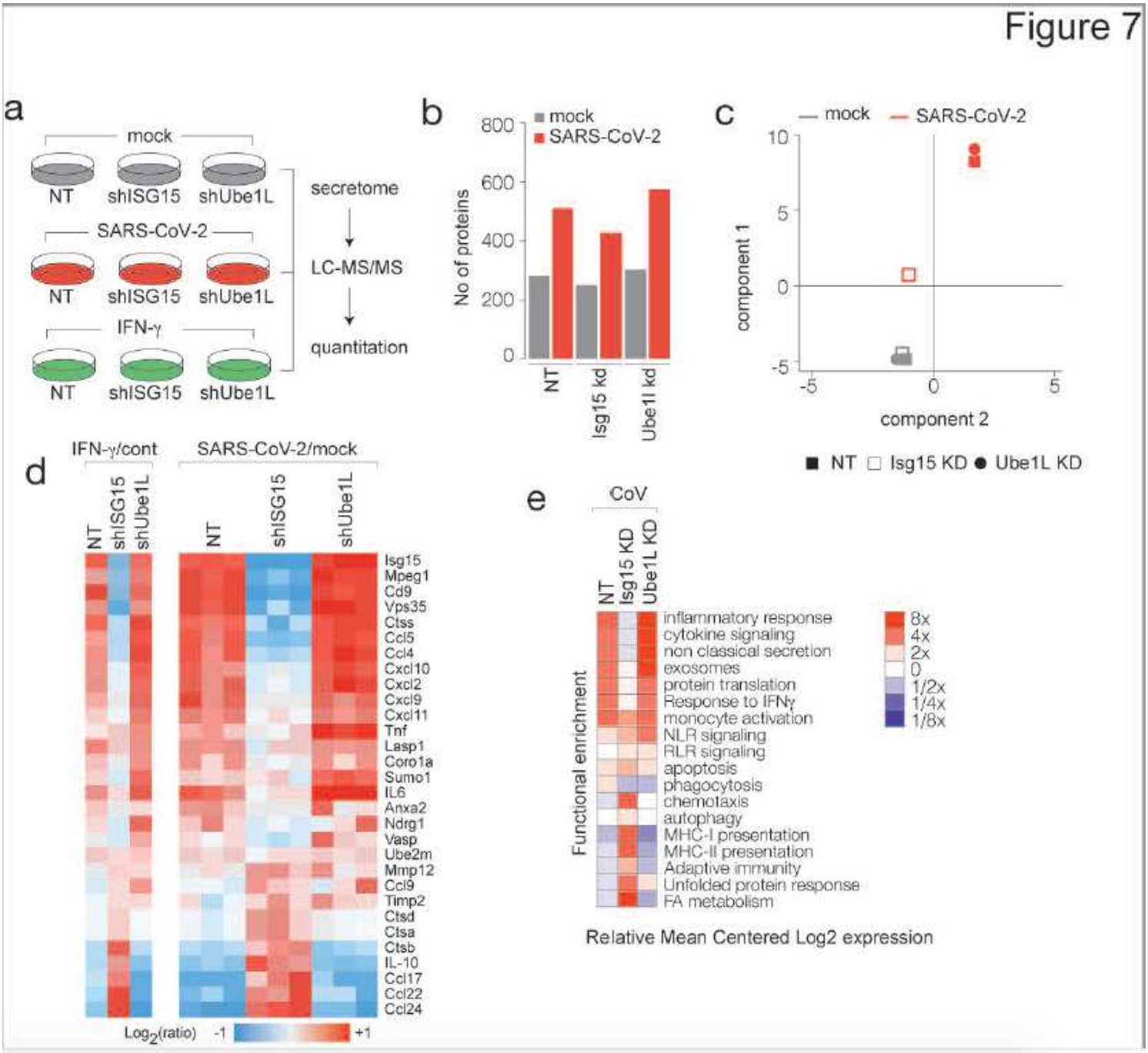

Figure 7

Quantitative analyses of ISG15-dependent responses in SARS-CoV-2 infected macrophages a. Schematic of the label-free strategy of LC-MS/MS used to study the ISG15- dependent secretome of SARS-CoV-2 infected cells. iPSC-derived macrophages were either transfected with non-targeting DsiRNA or those targeting ISG15 or Ube1L. Conditioned media was collected from control, SARS-CoV-2 infected or IFNg treated cells. Proteins were extracted from each of the samples, separated by SDS-PAGE and digested with trypsin for LC-MS/MS as described in the Materials and methods b. Total numbers of proteins quantified in at least two biological replicates c. Principal component analysis was performed using the Perseus software. Filled squares represent control cells (NT DsiRNA), empty squares ISG15-depleted, filled circles Ube1L-depleted. The uninfected cells are shown in gray and infected cells are shown in red d. The heatmap represents the hierarchical clustering of the common proteins in the secretome for IFNg treated or SARS-CoV-2 infected cells. The color key represents changes (log2 scale) from dark blue indicating the largest decreases to red indicating the largest increases e. Functional annotation of the common proteins identified in all samples was performed by the DAVID software.

Supplementary Files

This is a list of supplementary files associated with this preprint. Click to download.

- Supplementaryinformation.pdf